



Modelling Approaches for Aerospace Applications

Assignment

Marc Barcelo
December 2019

MSc Aerospace Computational Engineering

Index

Abstract.....	5
Introduction.....	5
Theory Fundamentals	7
· Equations	7
· Shock Waves Theory.....	7
· Aerodynamic Problem	10
Characteristics of the Problem	11
Results	14
Conclusions	28
Appendix 1: Finer Mesh Study.....	31
Appendix 2: Figure Detail.....	38
Appendix 3: Digitalized Experimental Data from (SCHMITT and CHARPIN, 1979), Case 2307.	
.....	42

List of Figures

Figure 1. Adhered/Detached Shock Wave depending on δ	9
Figure 2. Sections of the ONERA M6 Wing.....	12
Figure 3. Section 1, pressure coefficient distribution for the 5 turbulence models.....	14
Figure 4. Section 3, pressure coefficient distribution for the 5 turbulence models.....	15
Figure 5. Section 7, pressure coefficient distribution for the 5 turbulence models.....	16
Figure 6. Pressure Coefficient Distribution in each section.....	18
Figure 7. Pressure coefficient distribution in Section 4.....	19
Figure 8. Mach Contours in the upper wing surface (wall region)	20

Figure 9. Pressure Coefficient distribution along the wing and in each section.....	21
Figure 10. Pressure coefficient 3-D flow representation over the wing. Wing-tip detail	22
Figure 11. Pressure Coefficient contours in section 1 (the one it reaches highest values).....	22
Figure 12. Mach Distribution in all the sections.....	24
Figure 13. Velocity Magnitude Vectors in Section 5.....	25
Figure 14. Mach envelop X-Y Chart for each section	25
Figure 15. Shock waves captured in section 5. Illustration of the pure subsonic flow.....	26
Figure 16. Wing: Vortical Structures for Q-Criterion 0.001.....	27
Figure 17. Convergence of Errors in Refinement Case 1	31
Figure 18. Refinement Case 2. Cell Refinement.....	32
Figure 19. Error convergence of Case 2	32
Figure 20. Pressure Coefficient Distribution in Finer Mesh	34
Figure 21. Mach Contours of all sections for Finer Mesh.....	36
Figure 22. Up and lateral (from the wing tip) perspectives of vortex prediction, Q-criterion q=0.001.....	37
Figure 23. Boundary Layer widening.....	37
Figure 24. Residuals of the Coarser Mesh.....	38
Figure 25. Pressure coefficient distribution for Section 1, Coarse Mesh.....	38
Figure 26. Pressure coefficient distribution for Section 2, Coarse Mesh	39
Figure 27. Pressure coefficient distribution for Section 3, Coarse Mesh	39
Figure 28. Pressure coefficient distribution for Section 4, Coarse Mesh	40
Figure 29. Pressure coefficient distribution for Section 5, Coarse Mesh	40
Figure 30. Pressure coefficient distribution for Section 6, Coarse Mesh	41
Figure 31. Pressure coefficient distribution for Section 7, Coarse Mesh	41

List of Equations

RANS Mass Conservation (1)	7
RANS Momentum Conservation (2)	7
RANS Energy Conservation (3)	7
Shock wave Mass Conservation (4).....	8
Shock wave Momentum Conservation (5).....	8
Shock wave Energy Conservation (6).....	8
Shock wave Pressure Relationship (7).....	8
Shock wave Density Relationship (8)	10
Shock wave Temperature Relationship (9).....	10
Prandtl Condition (10)	11

List of Symbols

Re:	Reynolds number	e:	specific internal energy.
St:	Strouhal number	β :	incident angle of flow before the shock
M:	Mach number		wave
ρ :	Density	δ :	deviation angle after the shock wave.
p:	pressure	T:	Temperature
\bar{u} :	velocity field	a:	sound speed in current flow.
u_t :	tangential component of velocity	γ :	heat capacity ratio
u_n :	normal component of velocity	$\bar{\tau}$:	stress tensor
\bar{n} :	normal vector	$\frac{\delta}{\delta}$:	partial derivative
$d\sigma$:	differential surface, to be integrated	AoA:	Angle of Attack

Abstract

The purpose of this document is to evaluate the accuracy of numerical methods to predict and capture physical fluid dynamic phenomena over a wing in a transonic environment. The geometry to be evaluated is the well-known ONERA M6 Wing from which experimental data and results from similar simulations (Jakirlić et al., 2007) are available to compare and validate the results here obtained. Five different turbulence models - Spalart-Allmaras, Standard k-epsilon, Realizable k-epsilon, Standard k-omega, SST k-omega - will also be applied to determine its performance and high influence in the results. Furthermore, software used to run this simulation will be Ansys Fluent, and results will be treated with Ansys-CFD Post as well. At last, influence of the mesh quality in results will be equally examined by analyzing the coarse mesh and the effect of a refinement of the boundary region.

Introduction

We would like to start this document with a quote from one of the most privileged minds of the 20th century, Dr. Richard Feynman. He said “*there is a physical problem that is common to many fields, that is very old, and that has not been solved. It is not the problem of finding new fundamental particles, but something left over from a long time ago—over a hundred years. Nobody in physics has really been able to analyze it mathematically satisfactorily in spite of its importance to the sister sciences. It is the analysis of circulating or turbulent fluids.*”

This quote has remained truthfully until the current time this document is being written, yet turbulence remains abstract to human knowledge. Specially with the quick irruption and strong settlement of Computation Fluid Dynamics that propose interesting and considerably reliable solutions to the unsolvable Fluid Mechanics principles, several models have been created to capture -let's say, simulate - the complex fluid phenomena faced in physical and experimental environment.

The huge deviation noticeable if those models are compared, and the fact that none clearly outstands from others as the most trustworthy and advantageous at the same time, denotes the

strong need of where to focus the current investigation. This is why, particularly in fluid dynamics, results must be validated with empirical data withdrawn from expensive and accurate tests, which in some fields, is not that relevant to carry out.

Nonetheless, improvements in the accuracy of the numerical solutions are being made as time goes by. Enhanced versions of turbulent modelling, with corrections in equations and addition of numerical terms focusing the interesting effect to simulate, are normally applied hence the huge variety of available turbulence models. Current investigations suggest that further knowledge about the mysterious term of numerical diffusion must be achieved to complete the next big step in turbulence understanding and therefore modelling.

Following this idea, in the present document, the ability of academically widely used turbulence models to bare these phenomena will be analyzed and reviewed in consonance with data obtained through experimental tests. Thus, weak points in the particular model standard $k-\omega$ are expected to be obtained and then corrections of its internal variables can be proposed.

The geometry to be simulated and then, is a mesh of the Onera M6 semi-span wing, in the operation conditions of Mach=0.838 and Angle of Attack= 2.06°. Then, it will be compared to the Test 2307 carried out by (SCHMITT and CHARPIN, 1979) and to the research paper of: (Jakirlić et al., 2007) as well.

Theory Fundamentals

• Equations.

As it can be seen in the Assignment of “Validation and Verifications”, the fluid flux field will always be studied under the principles of mass, momentum and energy conservation. These, generally, are known to be the Navier-Stokes equations, which are correspondingly formulated in the following lines:

$$\frac{\partial \bar{\rho}}{\partial t} + \frac{\partial}{\partial x_j} (\bar{\rho} \tilde{U}_j) = 0 \quad (1)$$

$$\frac{\partial(\bar{\rho} \tilde{U}_i)}{\partial t} + \frac{\partial}{\partial x_k} (\bar{\rho} \tilde{U}_i \tilde{U}_k + \bar{\rho} \widetilde{u_i'' u_k''}) = - \frac{\partial \bar{P}}{\partial x_i} + \frac{\partial \bar{\tau}_{ik}}{\partial x_k} \quad (2)$$

$$\frac{\partial(\bar{\rho} \tilde{E})}{\partial t} + \frac{\partial}{\partial x_k} (\bar{\rho} \tilde{H} \tilde{U}_k + \bar{\rho} \widetilde{u_i'' u_k''} \tilde{U}_i) = \frac{\partial}{\partial x_k} (\bar{\tau}_{ik} \tilde{U}_i) - \frac{\partial}{\partial x_k} (\bar{q}_k + \bar{q}_k^{(t)}) + \bar{\rho} D_{kk} \quad (3)$$

However, the fact that the regime of operation is in transonic environment ($1 < M_\infty < 0.6$), additional physical phenomena and discontinuity in fluid magnitudes may take place. Hence, further physical-mathematical description and modelling must be done.

We will be mainly interested in the prediction of shock waves, which occur in local supersonic speed -then its huge presence in aerospace field - and will be detailed below.

• Shock Waves Theory

As it can be seen in (Landau L.D. and Lifshitz E.M., 1987), when the fluid field is determined by Navier-Stokes' equations, the fluid variables and their derivatives are always continuous functions in terms of space and time. Nonetheless, the same assumption cannot be if Euler equations are considered and conditions of high Reynolds number (Re) or Reynolds · Strouthal Number (Re · St) are faced.

This is because when terms relative to viscosity stress and heat flux proportional to temperature gradients are neglected or not considered, there is not any other available mechanism to eliminate the discontinuities of fluid magnitudes nor their derivatives.

However, the cutoffs of fluid variables (0-order discontinuities or finite) and the ones relatives to their derivatives (superior-order discontinuities or weak) are not arbitrary, since it is required that the conservation principles seen above are satisfied at any point.

In order to quantify the discontinuities, and according to the normal nomenclature, the fluid parameters will be evaluated before and after a discontinuity surface:

$$\rho_1 \cdot u_1 \cdot \bar{n} - \rho_2 \cdot u_2 \cdot \bar{n} = 0 \quad (4)$$

$$[(\bar{p}_1 \cdot \bar{n} + \rho_1 \cdot \bar{u}_1 \cdot (\bar{u}_1 \cdot \bar{n})) - (\bar{p}_2 \cdot \bar{n} + \rho_2 \cdot \bar{u}_2 \cdot (\bar{u}_2 \cdot \bar{n}))] \cdot d\sigma = 0 \quad (5)$$

$$\left[\left(p_1 + \rho_1 \cdot \left(e_1 + \frac{1}{2} \cdot u_1^2 \right) \right) \cdot (\bar{u}_1 \cdot \bar{n}) - \left(p_2 + \rho_2 \cdot \left(e_2 + \frac{1}{2} \cdot u_2^2 \right) \right) \cdot (\bar{u}_2 \cdot \bar{n}) \right] \cdot d\sigma = 0 \quad (6)$$

Regarding (5), if both terms are equal, there is no mass flux in the discontinuity surface—hence it is a so-called “fluid surface”. Derive from this fact a lot of kinematic properties that will not be discussed in here. Furthermore, as it can be proven in (Landau L.D. and Lifshitz E.M., 1987), the normal component of velocity (\bar{u}_n) is 0, (consequently they are called tangential discontinuities) and pressure is continuous, but the other magnitudes may not be at all. These surfaces can be considered as infinitesimal vorticity layers. Those tangential discontinuities are specially relevant in aerodynamics, being the base of the airfoil lift theory and finite-span wing.

In the other hand, if there is mass flux through the discontinuity surface, the velocity in normal component is discontinuous such as thermodynamic variables from (6), although tangential components will be in this case continuous. These discontinuities are known as “shock waves”, and as we have seen before they take place in supersonic operating conditions. Overall, they will affect the mean flow by increasing the static pressure and temperature of the mean flow but will decrease its velocity. Thus, $p_2 > p_1$, $T_2 > T_1$ and $u_{2n} < u_{1n}$ should be expected. The most important expressions of the relations before/after the shockwave are:

$$\frac{p_2}{p_1} = \frac{2 \cdot \gamma \cdot M_{1n}^2 - (\gamma - 1)}{(\gamma + 1)} \quad (7)$$

$$\frac{\rho_2}{\rho_1} = \frac{(\gamma + 1) \cdot M_{1n}^2}{2 + (\gamma - 1)M_{1n}^2}; \quad \frac{u_{2n}}{u_{1n}} = \rho_1 / \rho_2 \quad (8)$$

$$\frac{T_2}{T_1} = \frac{p_2}{p_1} \cdot \frac{\rho_1}{\rho_2} \quad (9)$$

Depending on flow conditions and geometries, several types of shock waves can be deduced:

- **Normal Shock Wave** ($u_t=0, \beta=90^\circ, \delta=0$)

- **Oblique Shock Wave** ($u_t \neq 0$, then β and δ can have any value). Their equations are the same as Normal Shock waves except for adding the relationship $\delta = f(M_{1n}, \gamma, \beta)$.

Special mention should the Prandtl Condition have here (see (Landau L.D. and Lifshitz E.M., 1987)) since it describes conservation of parameters through the shock wave. This factor will give us the idea of the behavior of the shock wave-boundary layer interaction. According to (eq), this relationship must be conserved along the flow:

$$u_{1n} \cdot u_{2n} = u_{1n}^2 \cdot \frac{\rho_1}{\rho_2} = \frac{2 \cdot a_o^2 - (\gamma - 1) \cdot u_t^2}{\gamma + 1} \quad (10)$$

It would also be interesting to briefly mention the most essential traits of weak shock waves as they normally take place in transonic – low supersonic regimes. The fact that the incident Mach is really close to 1, makes the term $M_{1n}^2 \approx 1$ and then (7), (8), (9) can be linearized. Flux is subsequently considered to be isentropic.

Another attractive endeavor to comment is, as we have seen before, the great influence geometry causes on the shockwave. If the geometry has a variation of angle $\Theta < \delta_{max}$ being δ the deflection of the flow after the shock wave, the shock wave is likely to adhere to the geometry surface. On the other hand, if Θ is greater than δ_{max} , the shock wave will be detached from surface as we will see in:

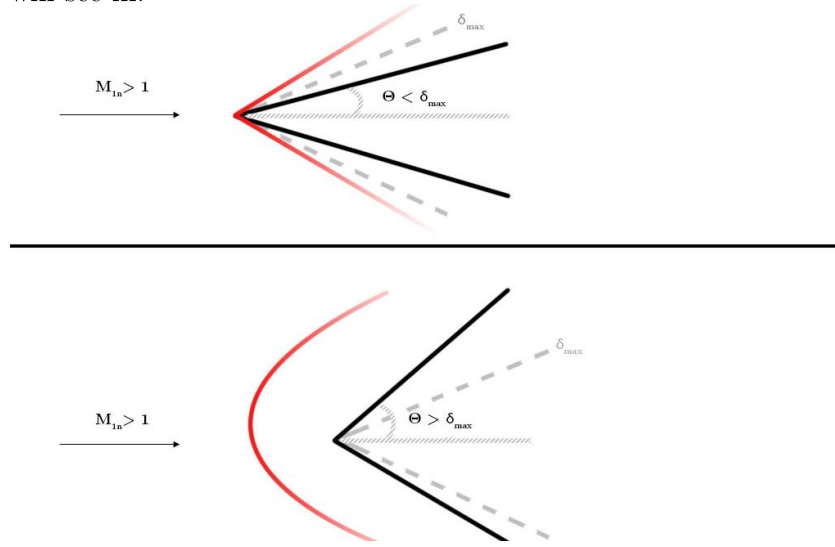


Figure 1. Adhered/Detached Shock Wave depending on δ

These are the most basic structures we will try to capture in our simulation. Their existence, nonetheless, implies a huge physical interaction with the mean flow and other structures (boundary layer, vortical structures, Prandtl-Meyer expansions, etc) which are not easy to identify nor to analytically describe, and even more difficult to simulate. However, according to aerodynamic theory of transonic regions, we know how the flow should look like and which phenomena are expected to take place. Then, in the following section, an introduction to the physical mean flow's characteristics will be given.

• Aerodynamic Problem

Serve this sector as a big picture of what we, a priori, should expect from the experimental and numerical results of the flow over the wing. Usually, due to the 2-D predominance of the effects (they tend to be “symmetrical” in the inner region of the wing) a flow over an airfoil section will be analytically studied.

As the airfoil faces the mean flow, the flow gets accelerated in its upper surface and then pressure decreases, which is one of the main parts of lift mechanism. When the environment is primarily transonic, for a particular M_∞ value, $M=1$ is reached somewhere in the nearby front part of the airfoil. This effect is known to be critical state -if not, it cannot be considered as transonic flow- from which critical values of the flow are withdrawn. Thus, a supersonic region appears immersed in the primary subsonic flow.

Furthermore, if we take a look at the supersonic “critical” region, iso-surfaces of “constant” Mach can be noticed due to expansion zones, and then they usually get closed by a shock wave - although Ignacio Da Riva, relevant aerodynamics professor in the late 60's, pointed out “*experience demonstrates that an isentropic continuous deceleration could also take place*”. If Mach number of the flow M_∞ is higher enough, expansion regions can be observed from the front to the tailing edge of the airfoil and even in the lower surface.

The position of shock wave will primarily depend on this Mach number, getting closer to the tailing edge as Mach is increased.

Nonetheless, it is also pertinent to talk about the adverse pressure gradient in the shock wave, which rapidly thickens the boundary layer and can make it detach if M is high enough. If

this effect occurs, drag is vividly increased and lift decreased in a similar way. That is what happened when the first tests of breaking the “sound barrier” catastrophically failed. This restraint has not been really overcome, since it is one of the parameters that limit the cruise operation of current aircrafts.

When the transonic problem is aimed to be described mathematically, the theory of potential linearized airfoil (and Prandtl-Glauert’s analogy)– which is widely used in pure subsonic and supersonic flows– does not describe accurately the physical phenomena that takes place. It can be seen in ((Liebeck and Langebartel, 1968)) that when c_p in the compressible scenario is calculated from the incompressible c_p , for $M_\infty = 1$, it tends to infinite which is not possible in reality at all. Then, this non-linearity states the need of using other complex approaches (usually using Finite Element Methods) with numerical algorithms.

However, the achievement of this step led to the creation of supercritical airfoils, which are widely used in current subsonic high-speed aircraft. An example of it, is the classic and well-known Harrier aircraft’s wing geometry.

Characteristics of the Problem

In the following pages, an evaluation of the simulation and numerical results for a transonic flow over the ONERA M6 wing will be described. Furthermore, the operation conditions and approaches made to acquire this solution have been the following:

Physical
freestream
conditions

$$\left\{ \begin{array}{l} M=0.838 \text{ (will be considered as } M_\infty) \\ \text{AoA}= 2.06^\circ \\ T_\infty= 300 \text{ K} \\ P_\infty= 101325 \text{ Pa} \end{array} \right.$$

Numerical
Assumptions

$$\left\{ \begin{array}{l} \text{Model: Density-based (Compressible Flows)} \\ \text{Density: Ideal gas} \\ \text{Viscosity Approach: Sutherland law} \\ \text{Turbulence Models: Spalart-Allmaras, Std and SST k-}\omega, \text{ Realizable and Std k-}\varepsilon. \\ \text{Solver: Implicit ROE-FDS, 2^{nd} Upwind order in Flow and 1^{st} in k, epsilon and omega.} \end{array} \right.$$

The tridimensional mesh used to simulate the flow around ONERA M6 wing has been given and it is not created by the author of this document. It contains a total of 294912 cells grouped in 4 fields: far field, interior fluid, symmetry, and the physical wing (named as “wall”). However, as results may suggest in the following pages, a refinement could lead to more accurate results and it has been performed as it will be seen.

As it has been said in Abstract, the main idea of this research is to determine how accurate are numerical methods to predict physical fluid dynamics phenomena but the influence of the turbulence model in the results as well. Thus, the data obtained simulating with Ansys-Fluent software will be compared to experimental results presented by (SCHMITT and CHARPIN, 1979) corresponding to the case 2307.

In this last document, the flow around 7 sections of the wing (through pressure transductors) has been described through the collection of pressure coefficient values along the dimensionless parameter x/c . Then, it will be necessary to evaluate the tridimensional fluid field in the exact same sections. To achieve this, 7 iso-surfaces (actually 14, 7 for wall and 7 for int fluid) will be created as the following Figure 2 reveals. Note them as white lines of the 3-D contour.

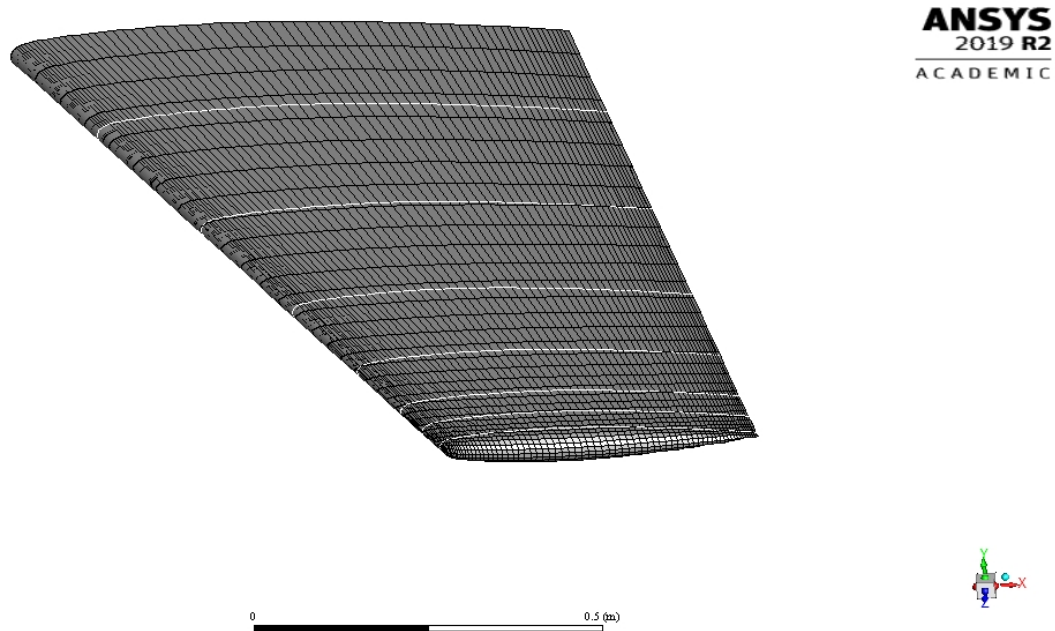


Figure 2. Sections of the ONERA M6 Wing

Further information about each section will be presented in the following table.

Table 1. ONERA M6 Wing Section Information

Section	% of b parameter	Position in Z axis
Section 1	20 %	Z=0.23926 m
Section 2	44 %	Z=0.52673 m
Section 3	65 %	Z=0.7776 m
Section 4	80 %	Z=0.95704 m
Section 5	90 %	Z= 1.07667 m
Section 6	95 %	Z=1.1365 m
Section 7	99 %	Z=1.184337 m

Precise information about each turbulence model has been already described in the previous “Validation and Verification Assignment”. For further knowledge, please consider reviewing the information of that assignment. However, as it will be seen in advance, the turbulence model that is expected to have better results in flow description is the SST k-omega as it merges the strengths of the k-epsilon model (good performance in mean flow) and from k-omega (good performance in boundary layer). Then, deeper analysis in the results and prediction of fluid dynamic phenomena in the most appropriate turbulence model will be seen in advance.

Results

• Turbulence Models

The solutions of each turbulence model in Sections 1, 3 and 7 will be displayed in Figure 3 by representing the pressure coefficient distribution along the x/c parameter in the limit sections and the intermediate one. With those three sections flow in the ONERA M6 wing will be characterized in a big picture. Then, a choice of the most accurate one will be done considering results of Figure 3 in order to describe with the most possible accuracy all the phenomena that can be numerically predicted through simulations of this kind - RANS.

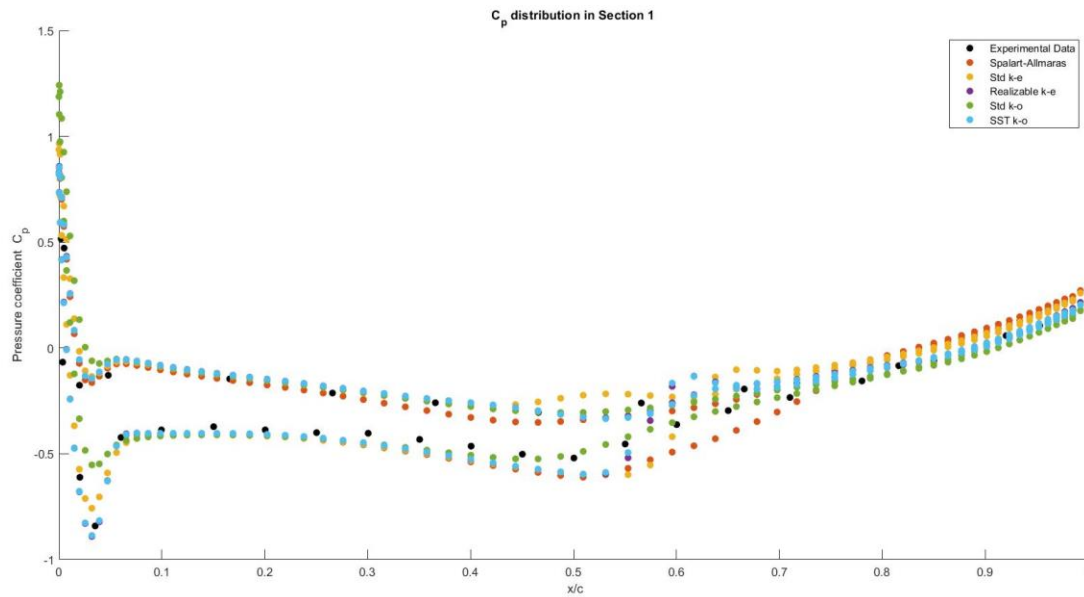


Figure 3. Section 1, pressure coefficient distribution for the 5 turbulence models

Figure 3 shows a really alike behavior for all the pressure coefficients. There's little deviation from one another. What can be seen, is that the SST k-omega model captured with more intensity the two shockwaves that will take place in the top and the bottom of the "airfoil" section. Nonetheless, the ones that displayed more accurate results have been: k-omega standard and then, the Spalart-Allmaras model. However, as it can be noted, the choice of one or another would not make a huge substantial change in the prediction of the flow.

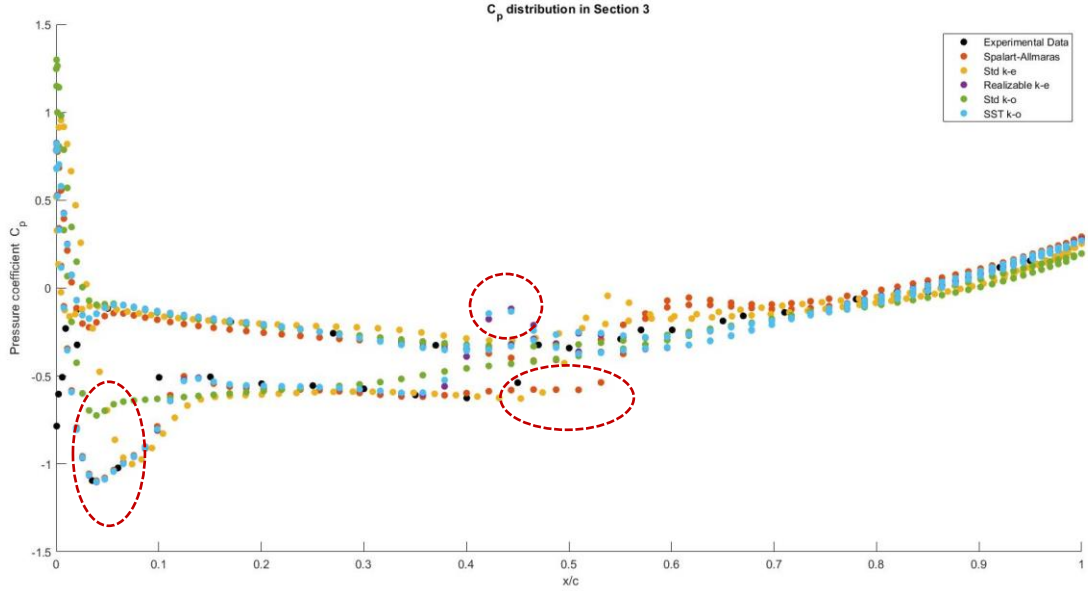


Figure 4. Section 3, pressure coefficient distribution for the 5 turbulence models

Now, Figure 4 reveals a different but interesting trait. The flow in section 3, which is one of the closest regions to half the wing and then entails the solution for the intermediate flow, is again really similar in all the turbulence models. Notwithstanding, there's not one predominant turbulence model in terms of closest results to the experimental data. Quite each performs correctly in a certain region, such as SST that predicts the underneath flow greatly but then, with the realizable k-epsilon, captures a phenomenon that physically does not exist. The opposite case can be seen in the standard k-omega, that does not perform an accurate prediction in the leading edge underneath flow but then has accurate solutions as s/c parameter is increased. Then, depending on what is aimed, in this section the most appropriate turbulence model is one or another, yet none outstands in comparison with the other.

Finally, Figure 5 displays the same scenario. Each model has its strengths and weaknesses. The SST Model, which is supposed to be the most accurate in predictions, seems to capture with realizable k-eps phenomena that physically do not occur. Maybe the ones that showed less deviation with the experimental results have been Spalart-Allmaras and Standard k-epsilon, but as stated, they also have small issues at some point of the pressure coefficient envelope.

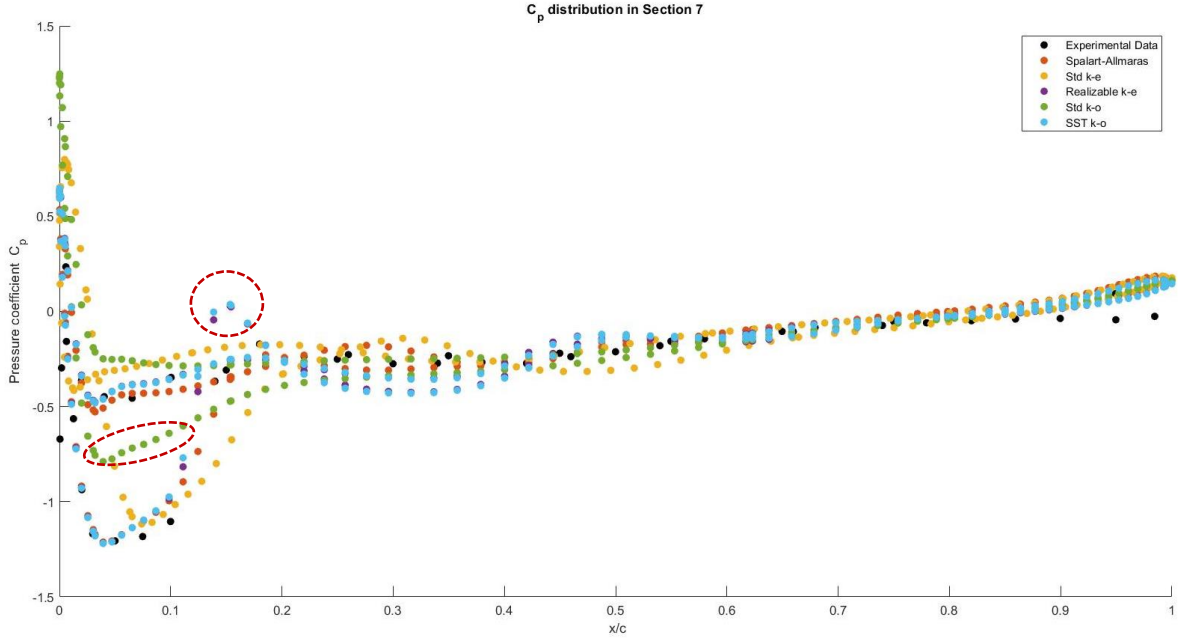


Figure 5. Section 7, pressure coefficient distribution for the 5 turbulence models

Overall, all the models behaved similarly and results seem to be acceptable at any case. Not a single method outstood in contrast with the other for the all the cases, then the choice of which is the most appropriate one is not clear. In the end, since this is an academic report and the intention is far more to learn than to extract the best solutions, and as there is not a single method that is better in all the environment, the Standard k-omega (which manages nicely the wall neighborhood phenomena in which we are interested) will be chosen to conduct a further study of the flow nature. This choice implies a really interesting idea: the results from this document and case (Case 2307, $M=0.838$, $AoA=2.06$) can be compared and contrasted to classmates whose case is the same one but probably performed Spalart-Allmaras – due to its quick results and wide application in aerospace- but also SST k-omega, which was expected to be the one with better approach to the physical phenomena. Besides, as it has been seen, the only point where the Standard k-omega was not that accurate is in the leading edge underneath flow, then this punctual weakness will be taken into account in the further study.

- **Standard k-omega Study**

For the mesh and flow conditions explained above, the numerical solutions of c_p along the x/c coordinate have been obtained and plotted against the experimental from (Jakirlić et al., 2007) for each section. They are assumed to be correct as errors “converged” -they remained constant at some point- for all the turbulence models (for the particular case of k- ω Standard see Figure 24 attached in Appendix 2: Figure Detail since it will be the model we will analyze the most). In this process, we had to face the issue that the numerical data was not in the same scale the experimental did -since it was in absolute x/c instead of relative- thence the MATLAB function of “resample” was used for the x axis.

In the following page we can see, overall, the 7 mentioned plots. However, a zoom in each will be recommended, and bigger graph of each can be seen in the section: Appendix 2: Figure Detail. Serve this appendix to display with large figures all the details that here can't be shown if a “continuous” and fluent document is chased, as large images may help reader to lose the continuity from the text explanation.

Figure 6 -at first glance- reveals two evident aspects: the experimental points of pressure coefficient are not enough to perfectly describe the pressure distribution along the section (airfoil). Some important information can be therefore omitted. In the other hand, overall, the numerical results show great similarity with the experimental envelope: predictions seem to be accurate. However, as x/c parameter is increased – as sections get closer to the wing tip- some deviations can be noticed in the plots. They, primarily, can be caused by the turbulent and vortical structures that are present in the physical wing but are not well captured by simulations and its approaches. Those differences will be later discussed with further post-processing and mesh refinement.

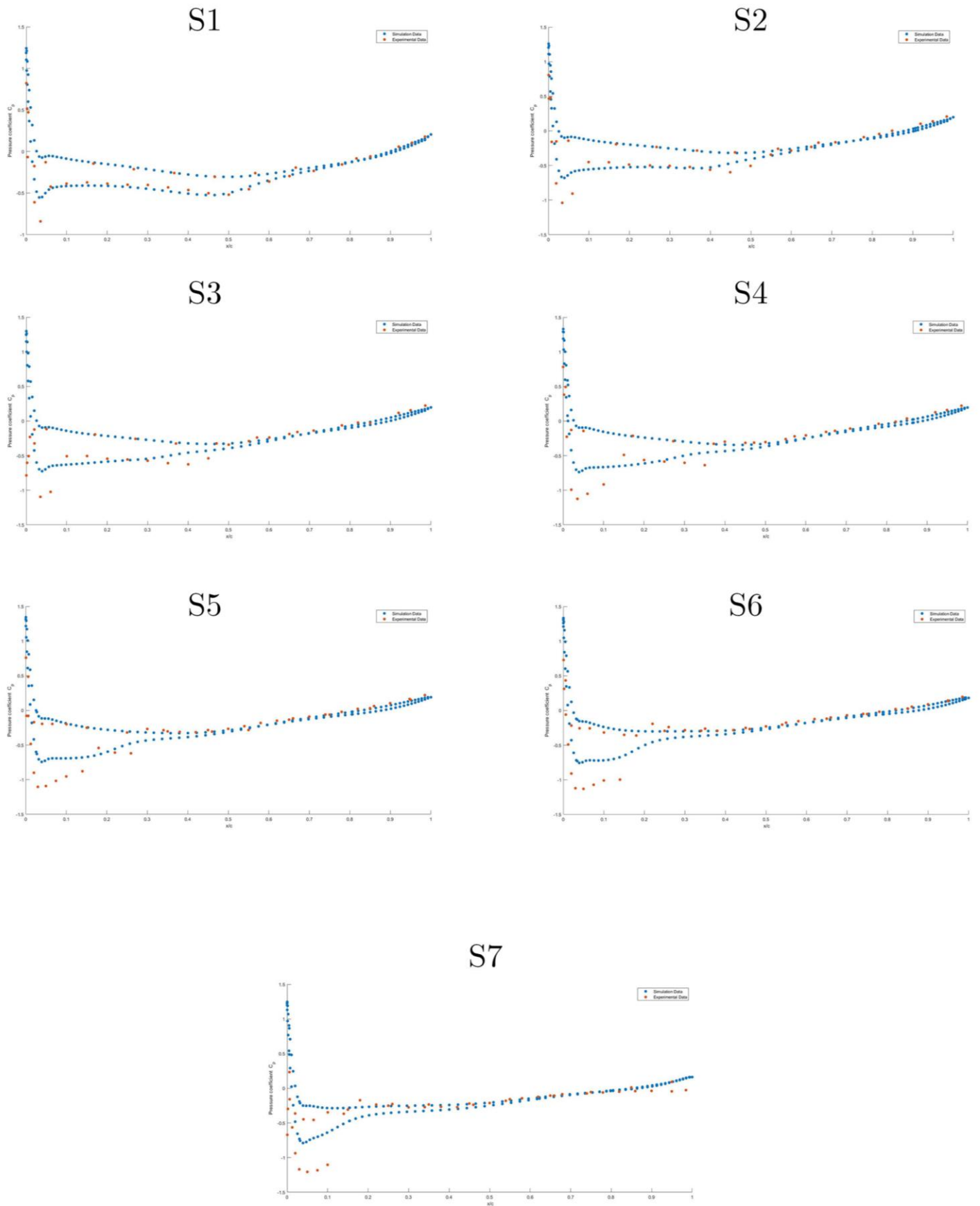


Figure 6. Pressure Coefficient Distribution in each section

It is also interesting to discuss the physical phenomena we can deduct from this graph. Please, serve the following image (Intermediate Section 4) as a generic to evaluate and then we will extrapolate deductions to the whole wing and analyze the x/c effect.

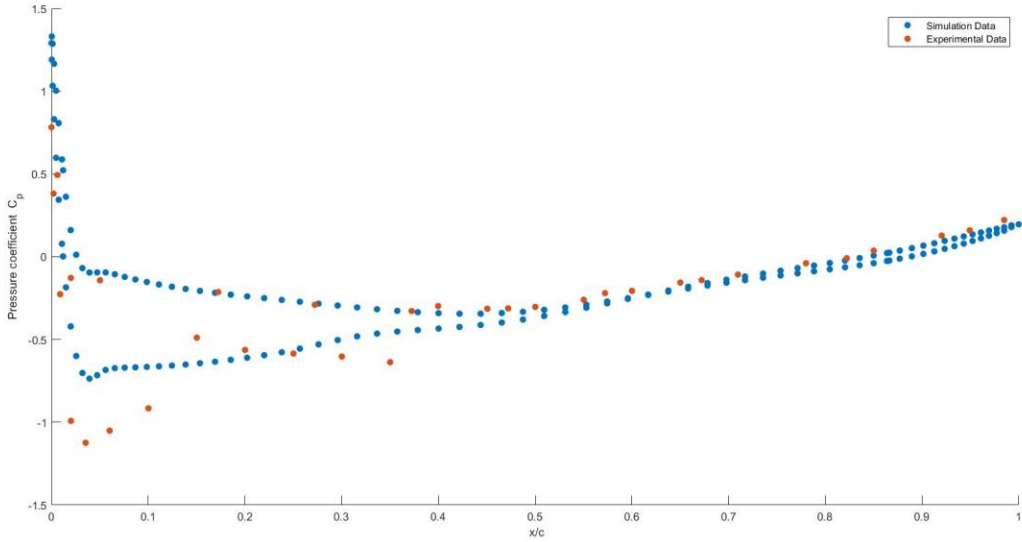


Figure 7. Pressure coefficient distribution in Section 4

As it was expected, flow pressure increases when it meets the leading-edge of the wing. Pressure is lower in the upper surface as flow speed rapidly increases, then the gradient of pressure between upper and lower faces of the airfoil will result in lift creation. It is also perceived how pressure coefficient suffers a decrease after the weak shockwave (local Mach barely overpasses 1.2) in the upper but also the lower region, which is more abrupt in the experimental data than the ones obtained in the simulation. Additionally, it is hard to tell but, in the tailing region, numerical results may suggest that there's a slight effect of possible tip vortexes predicted by the flow simulations. Boundary layer could perceive the first stages of detachment. Those, due to the few available data points from (SCHMITT and CHARPIN, 1979) cannot be fully compared with certainty and detail to experimental simulations. Nevertheless, they seem to be consistent with (Jakirlić et al., 2007), where this effect was noticed for the same wing but different operating conditions for a cord-section ratio of 0.99.

Nonetheless, more information of this case can be withdrawn from FLUENT Software and CFD-Post if other vector fluid magnitudes are evaluated. As it has already been remarked in the subsections · Shock Waves Theory and · Aerodynamic Problem as well, the Mach contours for the fluid region will provide us a deeper understanding of how flow operates.

We expect an “inverse” relationship between the Mach and pressure behavior. The wall will suffer from the maximum values of pressure and flow incidence in the leading edge of the wing. Figure 8 and Figure 9 will corroborate these grounded hypotheses.

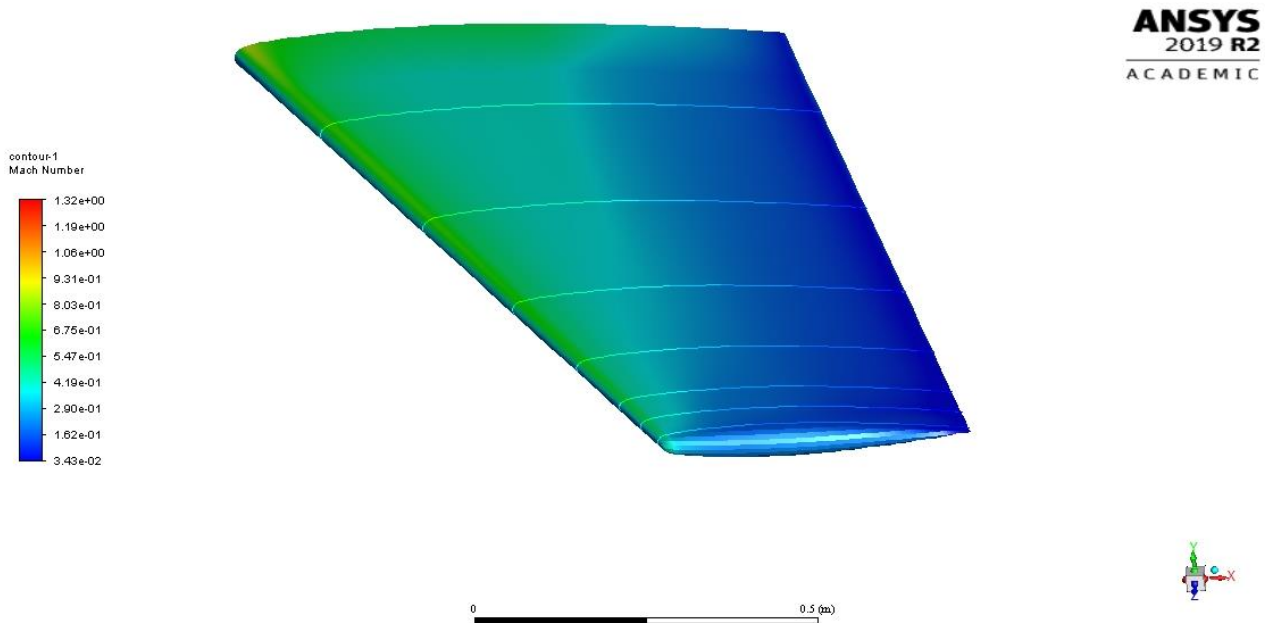


Figure 8. Mach Contours in the upper wing surface (wall region)

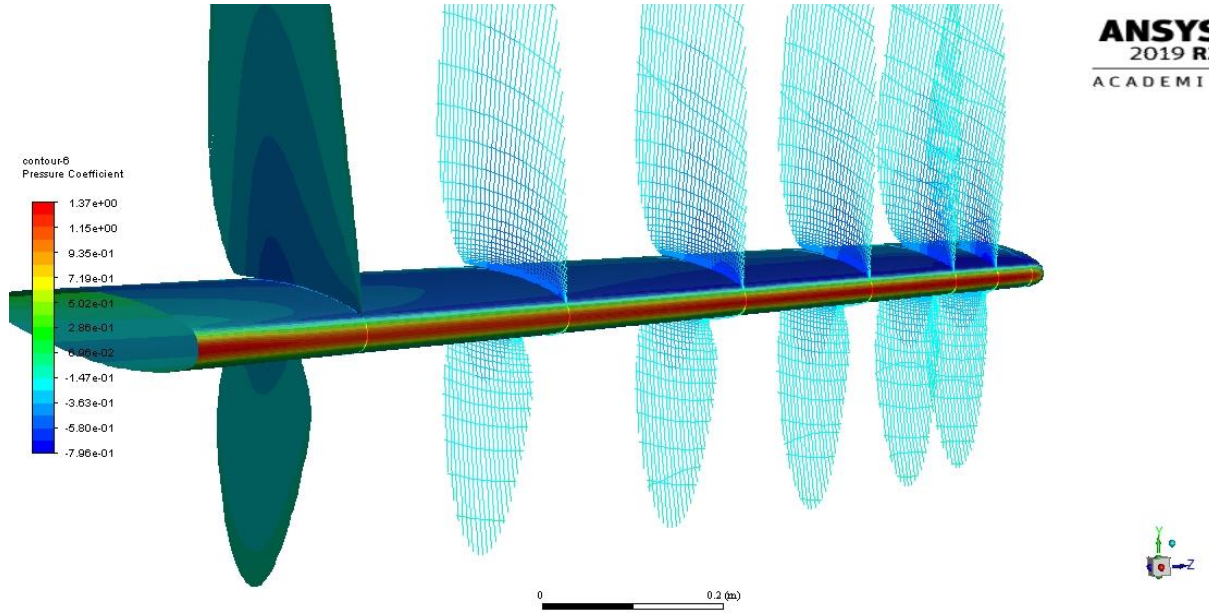


Figure 9. Pressure Coefficient distribution along the wing and in each section.

Specially Figure 9 demonstrates an excellent overview of the general flow. Nevertheless, as it can be seen, issues with Fluent have been had when representing sections 2-6 and a grid-like graph has been obtained, which may not be as clear as the filled section 1. It has not been solved, although interesting traits can be withdrawn anyway, and even further analysis will be made. Pressure is bigger in the leading edge than in the tailing edge as formulated, and more severe as it gets closer to the fuselage than the wingtip if the Z coordinate is analyzed. The pressure coefficient distribution in each section -where it achieves the minimum values- demonstrates the expansion zones of flow when it is close to the airfoil wall, and those zones increase in value as they reach the tailing edge. After those, they will reach higher values in a point close the tailing edge (due to our particular transonic flow nature of concrete M and AoA) once oblique weak shock waves take place in the upper and lower flow regions.

Not much more information can be sighted if Figure 9 is seen from the wingtip approach or pressure distribution of a section is examined, nevertheless, they could confirm our guesses. Then, serve Figure 10 ad Figure 11 as graphical confirmation of the phenomena explained above.

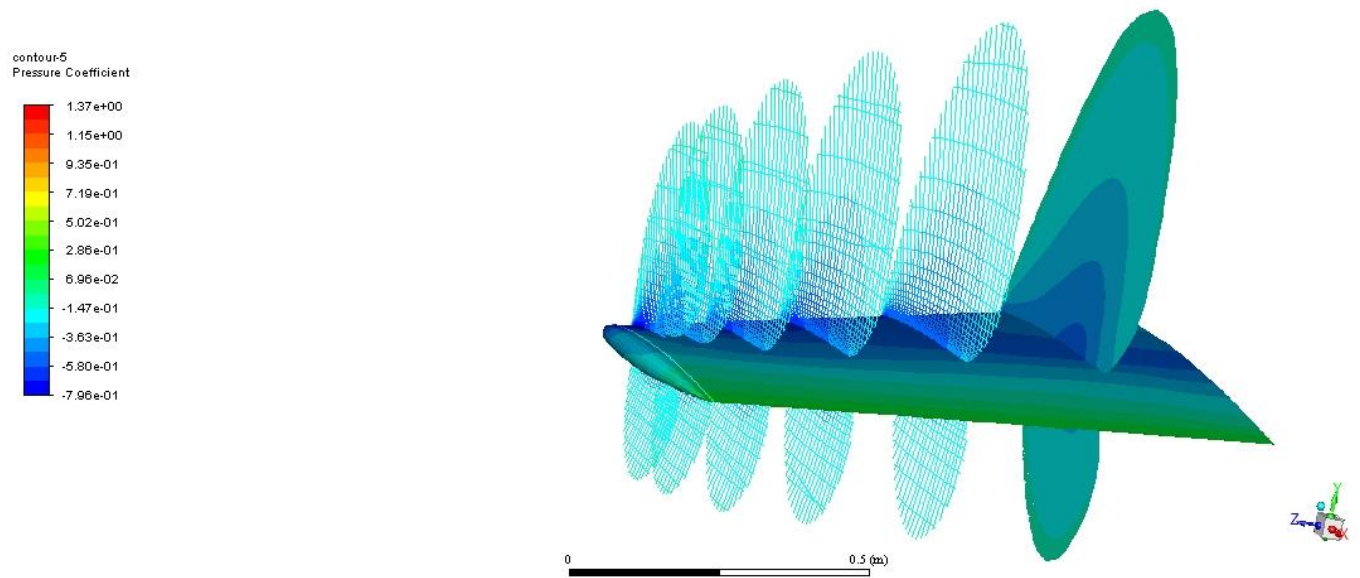


Figure 10. Pressure coefficient 3-D flow representation over the wing. Wing-tip detail

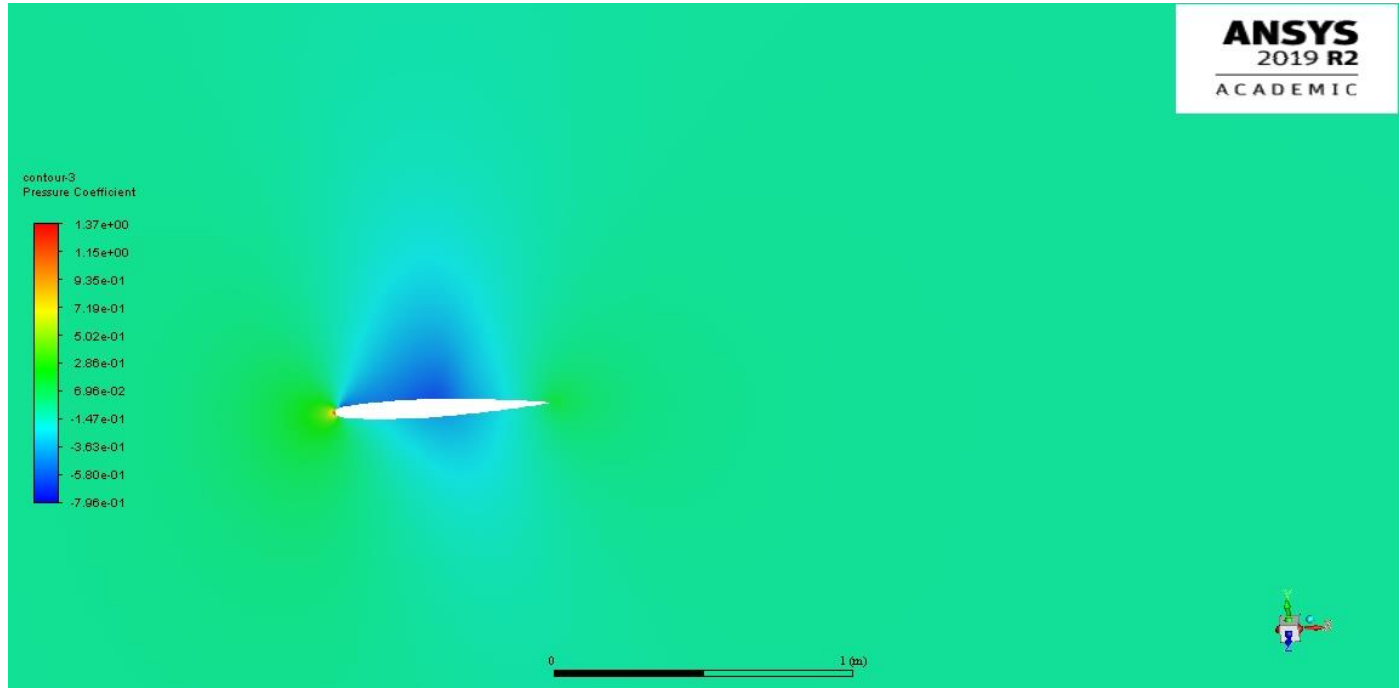


Figure 11. Pressure Coefficient contours in section 1 (the one it reaches highest values)

However, Mach contours can provide another useful insight into the flow nature and will show the complementary effects of the one perceived with pressure distribution. It is important to remind the reader that theory fundamentals of Mach and expected flow are already described in sections: · Shock Waves Theory and · Aerodynamic Problem and will not be explained again.

Figure 12 settles the interesting traits left to recognize. It reveals, as guessed, the inverse nature of the velocity-pressure field. But then a more sharp and accurate distribution of the flow can be perceived.

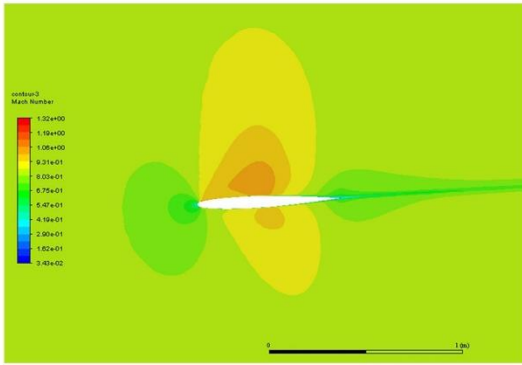
The issue with fluent we had in the pressure coefficient graph has not been solved neither here so the first surface was correctly obtained with Ansys-Fluent whilst the others -surface 2 to surface 7- were performed with CFD-Post. One or another have yet shown to be equally valid.

The supersonic immersed flow field in the subsonic general region demonstrates an evolution of the expansion zones as sections to the wing tip are examined. This supersonic region is higher near the fuselage, but it gets more intense in approximately intermediate regions such as sections 4, 5, 6, where the expansions seem to adhere to the wing surface. Mach distribution in advanced regions is seen to be lower probably due to the diffusion caused by wingtip vortical structures but also to the vicinity of the mean flow.

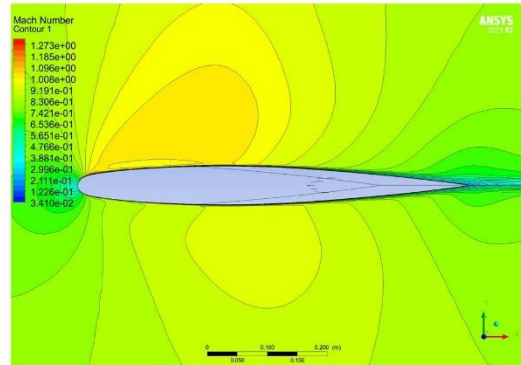
The oblique weak shockwaves that immediately finish those expansion zones are clearly seen as well. In the upper region one can be found at about 70% of the cord, yet there's also one in the lower surface starting at approximately 80% of the cord. If incident Mach M_∞ was increased, they would appear closer to the tailing edge until flow started to detach, and cruise operation would get compromised.

Initially, as we represented Velocity Magnitude Vectors in an arbitrary section -we chose section 5 as an intermediate one- its plot in Figure 13 made us think that there were really weak -almost unperceivable- detached shock waves in front of the leading edge as it could suggest and as it has been reviewed in · Shock Waves Theory.

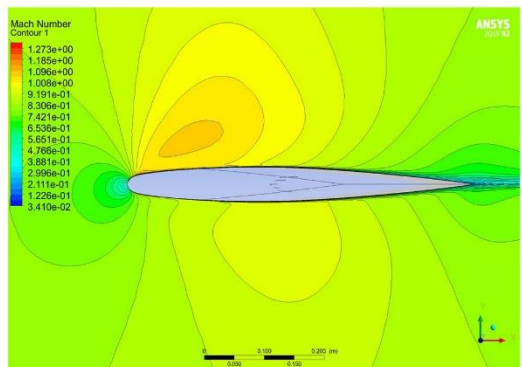
Section 1



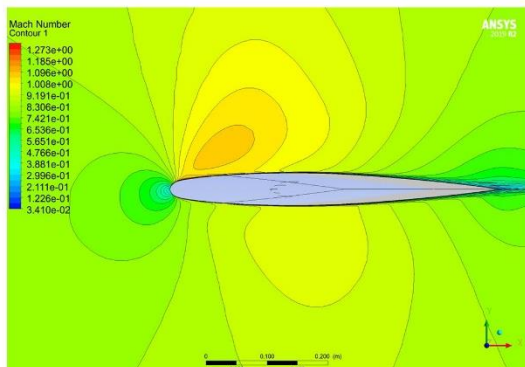
Section 2



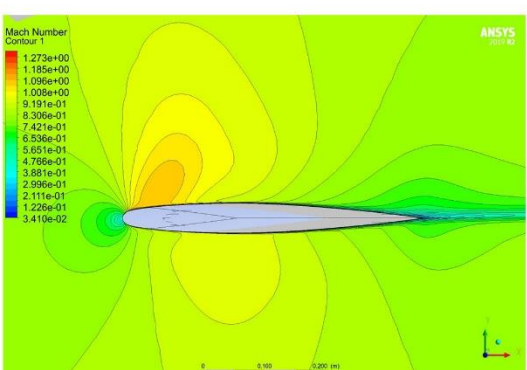
Section 3



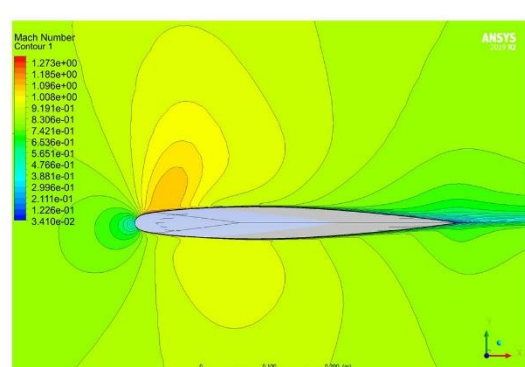
Section 4



Section 5



Section 6



Section 7

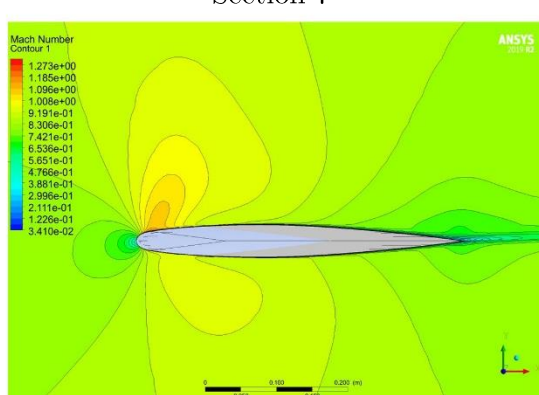


Figure 12. Mach Distribution in all the sections

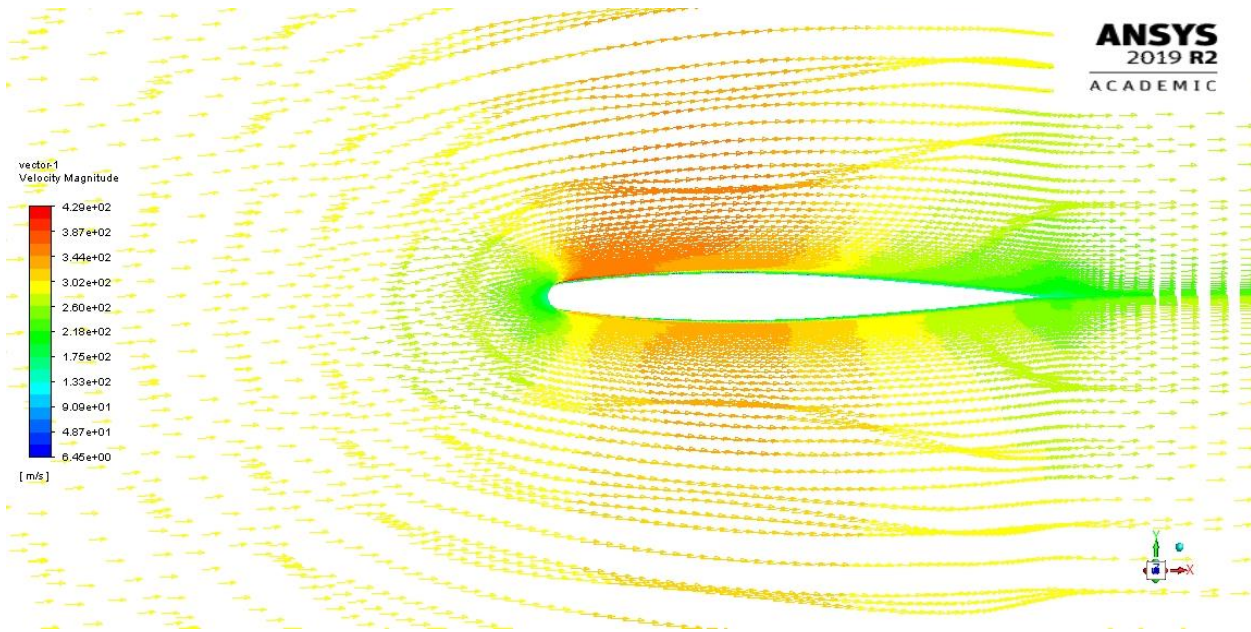


Figure 13. Velocity Magnitude Vectors in Section 5

Nonetheless, this hypothesis was rapidly discarded by representing the Mach envelop X-Y chart in each section as Figure 14 demonstrates how Mach 1 is uniquely obtained after the leading edge in the chord positions ($\sim 70\%$ and 80% for upper and lower surfaces regions respectively) we saw before.

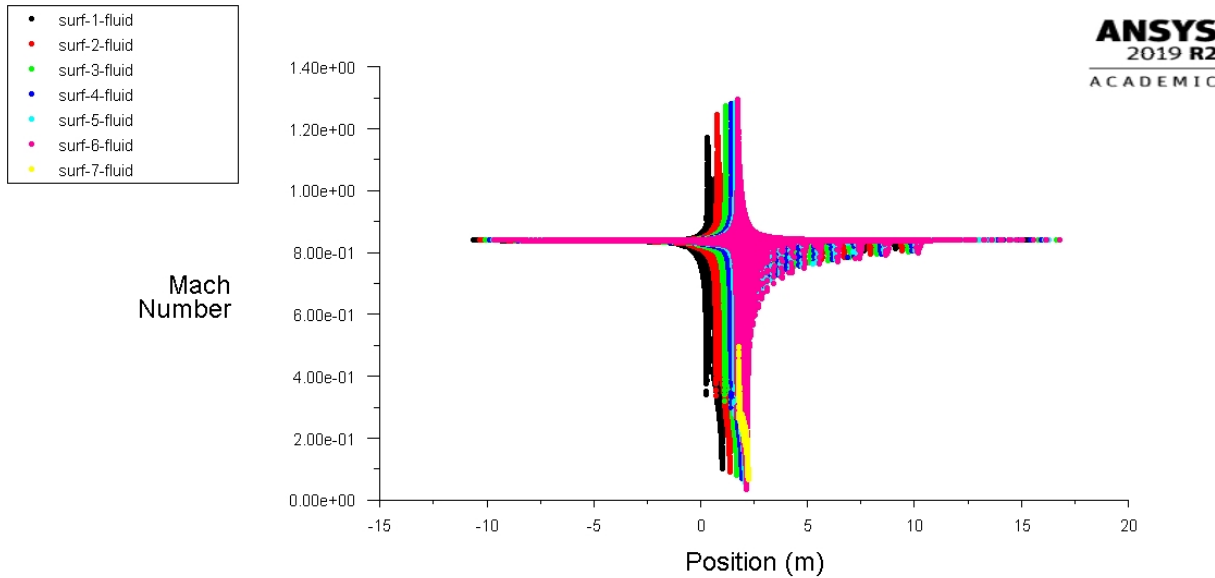


Figure 14. Mach envelop X-Y Chart for each section

Another interesting strategy to nicely capture the shockwaves is to create an iso-clip in Ansys-Fluent Software restricting the sections to subsonic behavior ($M < .95$ for example). Then, when evaluating an arbitrary section such as section 5, Figure 15 was obtained and only the pure subsonic flow is represented. Thus, the two expected shock waves have been accurately located.

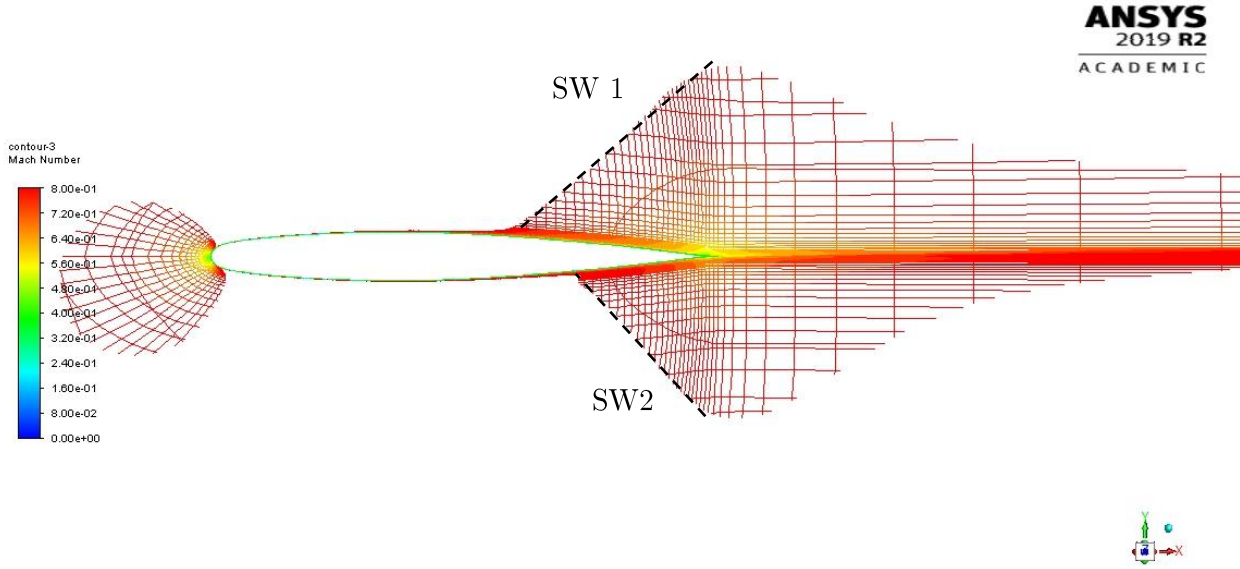


Figure 15. Shock waves captured in section 5. Illustration of the pure subsonic flow.

Nonetheless, to gain a further knowledge on the flow nature of the numerical solution, the vortex structures are also considered and plotted with the Ansys-CFD Post software. They are proven to have great influence in the flow behavior and to describe more complex phenomena (mixing layer, etc) not discussed in this document. Our approach has been with the Q-Criterion (see (Haller, 2005)), having a value of 0.01 to be able to determine the initial and stronger sources of vorticity. The results of this arrangement can be sighted in Figure 16.

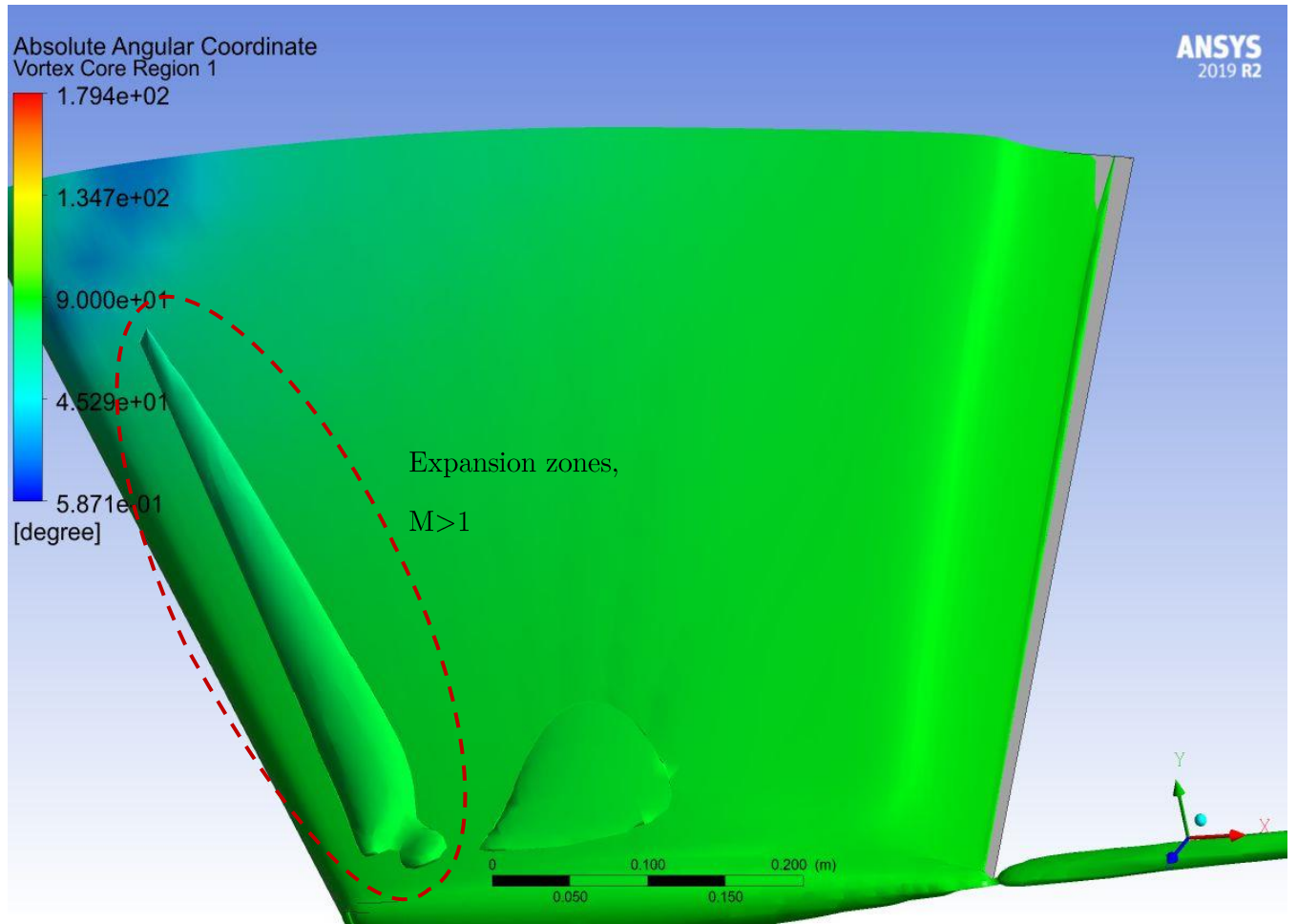


Figure 16. Wing: Vortical Structures for Q-Criterion 0.001

The need of performing a refinement in the boundary-region vicinity is again demonstrated. The illustration shows the upper region of the ONERA M6 wing seen from the wing tip. The only relevant phenomena it has been able to roughly represent is the expansion zones. This whole process will be repeated -with less explanation- in Appendix 1: Finer Mesh Study where more information can be withdrawn.

Conclusions

Overall, the results obtained with the numerical schemes, turbulence models and specially Standard k-omega turbulence model showed great concordance with what was expected from the fluid dynamics theory and with the experimental data provided by (SCHMITT and CHARPIN, 1979) as well.

Several phenomena such as weak oblique shock waves, expansion zones, boundary layer interactions and production of vortical structures have been clearly identified even though the Standard k-omega model applied (with no corrections) is not the most -nowadays- strong to numerically simulate all of them. As every turbulence models as it has been demonstrated, it has its own strengths and weaknesses. Besides, the transonic environment involves an added difficulty to the mathematical description since widely used theories (Prandtl-Glauert) that properly describe subsonic and supersonic regions, do not merge correctly both flow natures in the transition between them. But, this initial challenge has been rapidly solved with the satisfactory results.

Thus, a further step in flow dynamics' understanding can be done in contrast with traditional methods such as by applying potential theory and with expensive experimental test. Nonetheless, these last are still currently required to be carried out to understand how accurate are results from numerical schemes and to serve as a solid reference of the physical phenomena that takes place in the flow.

Due to all these reasons, the flow over the ONERA M6 could be sharply reproduced and therefore understood and described in the pages above.

Moreover, the effect of geometry of the mesh has also been evaluated by comparing both results from the given mesh and after performing refinement of its boundary layer. This step was not required, but it implied an interesting step to be performed. Once done, it has clearly been

demonstrated its great influence on the accuracy of the solutions and to the ability of the numerical method to predict or capture the physical that takes place.

The refinement of the boundary layer has been performed by Ansys-Fluent although it is not the most appropriate software to edit meshes. Proper software such as Ansys-Meshing and Pointwise have been tried to be used but the “.cas” data (although we exported a .mesh file) made it quite impossible to treat them with both software. Ansys-Meshing did only accept “.meshdat” extension files and Pointwise did not show all the regions and information needed to refine the fluid mesh. However, it has been finally completed with the Fluent software and results do not suggest any bad performance of it.

Additionally, experimental data from the (SCHMITT and CHARPIN, 1979) document has been tough to be extracted and digitalized since they are written by typewriter and several characters are easily confused. Applying OCR techniques do not make any substantial changes as computer is not able to understand those characters either. Then, this information has been digitally gathered in Appendix 3: Digitalized Experimental Data from (SCHMITT and CHARPIN, 1979), Case 2307. in case they are required for further students of this MSc, saving time and effort and avoiding confusions.

The present document leaves a lot of interesting work to be done. First, many other turbulence model can be examined, even the ones with corrections and even to propose a correction of the SST k-omega model that led to more accurate prediction of flow behavior, and then a comparison of their results would reveal the positive and negative traits of each model and which is more appropriate to predict flow nature. Experience says that generally, one of the most accurate and satisfactory models is the SST k-omega, that combines the strengths of standard k-omega and k-epsilon turbulence models. Moreover, Spalart-Allmaras is quite used as well due to its good performance and to its rapidness to present results. Then, the choice of the turbulence model entails a compromise solution between accuracy and computational cost.

Evidently, further knowledge in fluid dynamics and aerodynamics would be also interesting to acquire in order to recognize and understand more complex phenomena that takes place in the

flow and that has not been evaluated in the present document. And there are a lot of CFD concepts and approaches to be learnt and experienced as well, and that will be examined in the next modules and work. Nevertheless, I believe I achieved the objective of the assignment and I am satisfied with the work done.

References

- Haller, G. (2005) "An objective definition of a vortex," *Journal of Fluid Mechanics*, 525, pp. 1–26.
- Jakirlić, S., Eisfeld, B., Jester-zürker, R. and Kroll, N. (2007) "Near-wall, Reynolds-stress model calculations of transonic flow configurations relevant to aircraft aerodynamics," *International Journal of Heat and Fluid Flow*, 28(4), pp. 602–615.
- Landau L.D. and Lifshitz E.M. (1987) "Fluid Mechanichs," *Institute of Physical Problems, USSR Academy of Sciences*, 6
- Liebeck, R.H. and Langebartel, R.G.; J.R.P. (1968) "Optimization of Airfoils for Maximum Lift"
- SCHMITT, V. and CHARPIN, F. (1979) "Pressure distributions on the ONERA M6 wing at transonic Mach numbers"

Appendix 1: Finer Mesh Study

The results obtained in previous sections clearly state the need of performing a refinement of the mesh, although this process has not been easy to achieve. The results will be focused in analyze results exclusively from the same turbulence model (standard k-omega) to properly contrast them with the coarse mesh. In most of the simulations conducted, errors diverged at some point or where not accurate enough. Thus, added to the computational cost demanded for this simulation in comparison with the ones done so far, a lot of time has been invested until decent results have been obtained.

Four our operation conditions, two refinements of all the cases that have been tried led to proper solutions: first, a refinement of 40 normal cells to the wall function and a refinement level of 10. After 1 hour of running time, 276 iterations were done and errors seemed to converge as Figure 17 shows.

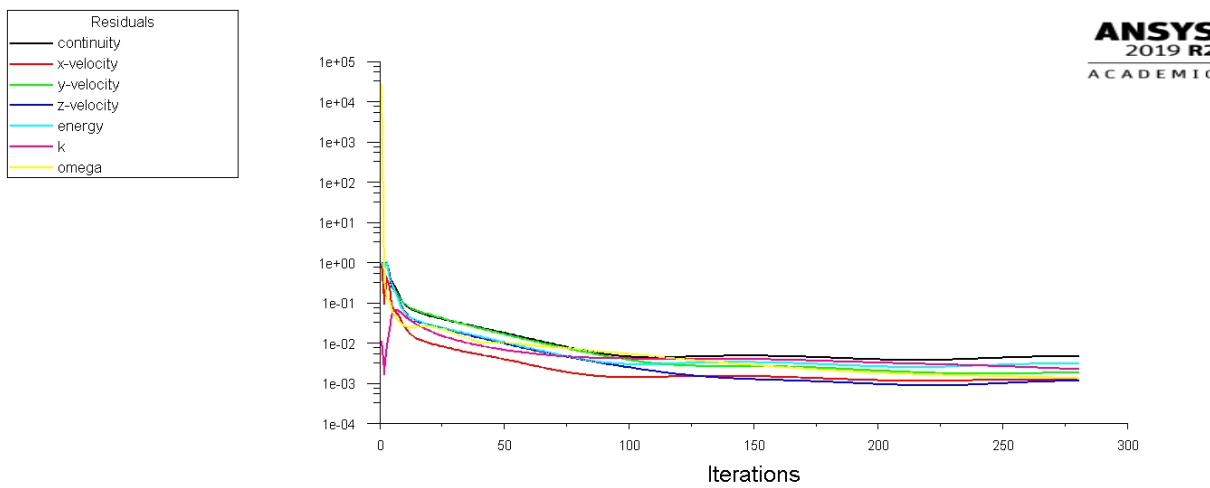


Figure 17. Convergence of Errors in Refinement Case 1

However, more interesting and less computational-demandant is the next refinement scenario: 20 normal cells from boundary layer, with a refinement factor of 4 - see Figure 18. This case, if Grid Convergence studied was performed, will be less prone to suffer from over-refinement and then more chances to be valid. Furthermore, errors have “approximately” converged correctly as Figure 19 demonstrates. Then, from both, this case will be deeply examined in the following pages.

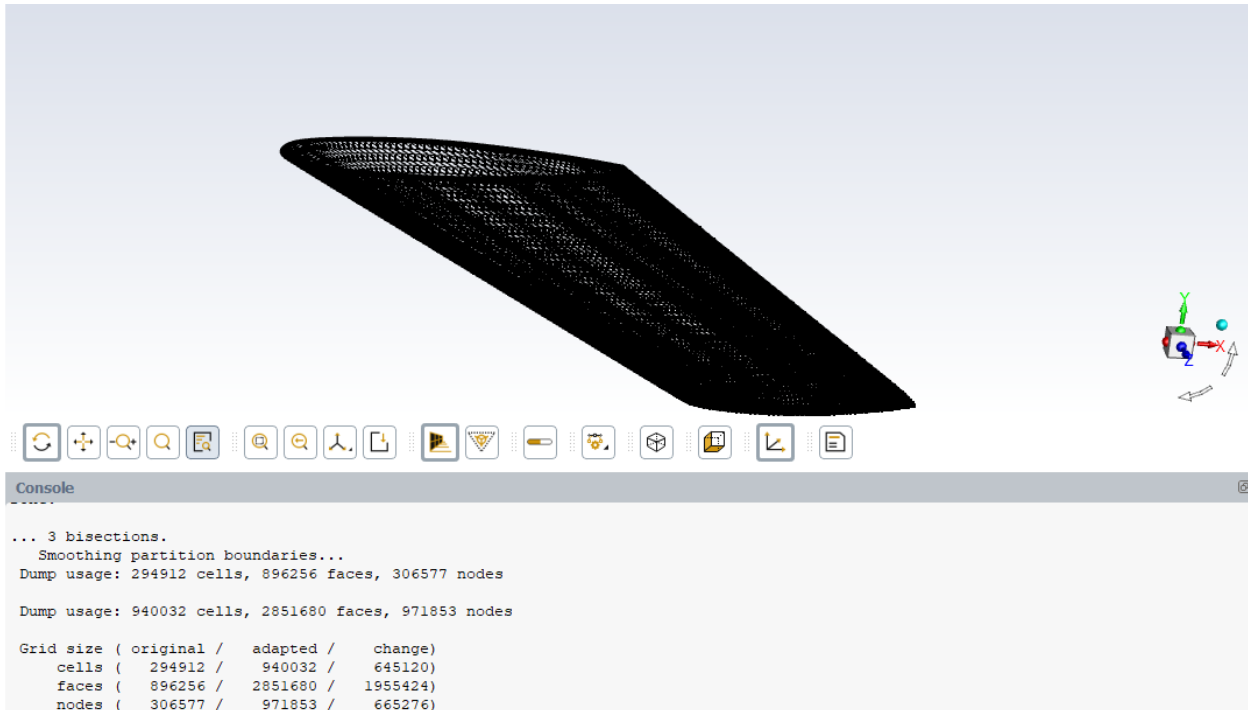


Figure 18. Refinement Case 2. Cell Refinement

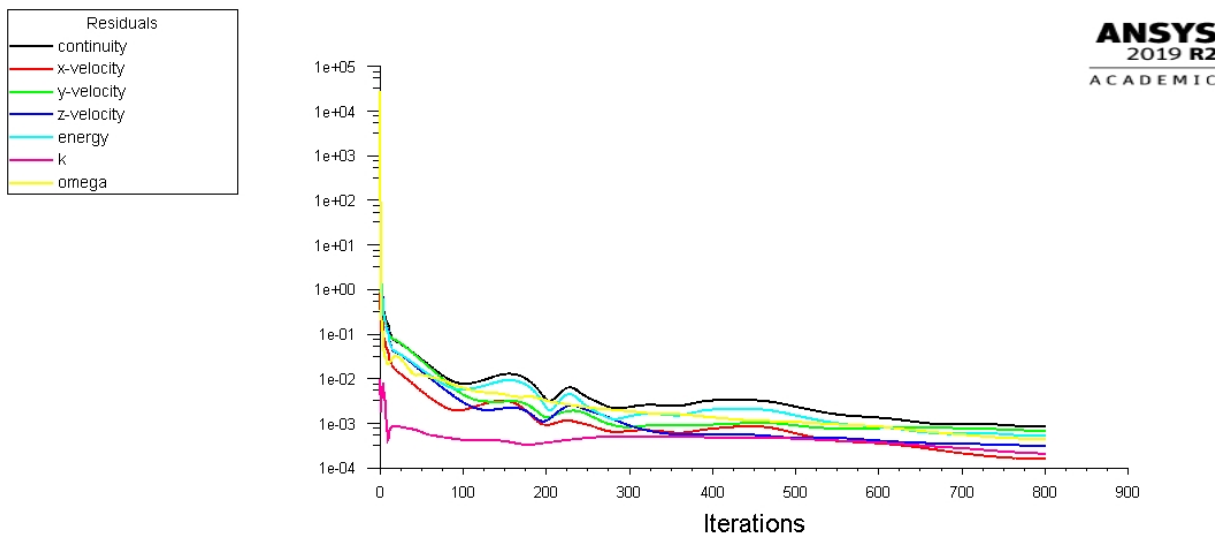


Figure 19. Error convergence of Case 2.

The operation conditions and numerical approaches are exactly the same as the study with the “coarser” or given mesh. In case it is needed to refresh them, we refer the reader to the section of: Characteristics of the Problem.

We will first analyze the coefficient pressure plot in comparison with the coarser mesh, and once seen that results are more than valid, additional phenomena from Mach contours will be tried to be deducted. Thus, the methodology applied will be equal to the one from Results section.

Figure 20 reveals some positive aspects but one potentially negative as well. As it can be seen, the number of points is increased then more information of the pressure coefficient distribution is available and can be contrasted. Then, the shock wave of each upper and lower regions can be clearly noted and captured in comparison with the coarser mesh nor the experimental data. Additionally, if section 7 is examined carefully, the influence of vortex structures in wing tip can be noted, which is consistent with the study of (Jakirlić et al., 2007).

Nonetheless, slight deviation from coarse and experimental data can be seen, although the general shape is really similar to both and there's no substantial change. Aerodynamical effects and fluid mechanic phenomena could be overpredicted. It must be yet considered that experimental data comes from (SCHMITT and CHARPIN, 1979), and transductors by that time were not as accurate and tiny as there are nowadays. Thence, their shape may introduce perturbations to the mean flow acting as if they were additional wall elements and therefore could be slightly different, more approached to the finer mesh. These deviations observed may also be exaggerated by the fact that experimental data collected is not large enough to accurately plot the flow distribution over the section (airfoil). Then, bearing in mind all the pros and cons described here and noted in Figure 20, we will keep moving with results. If the variable $Y+$ was examined in both simulations performed so far, we would be more certain about each's accuracy. However, this variable is yet unknown to us and will be understood in next modules.

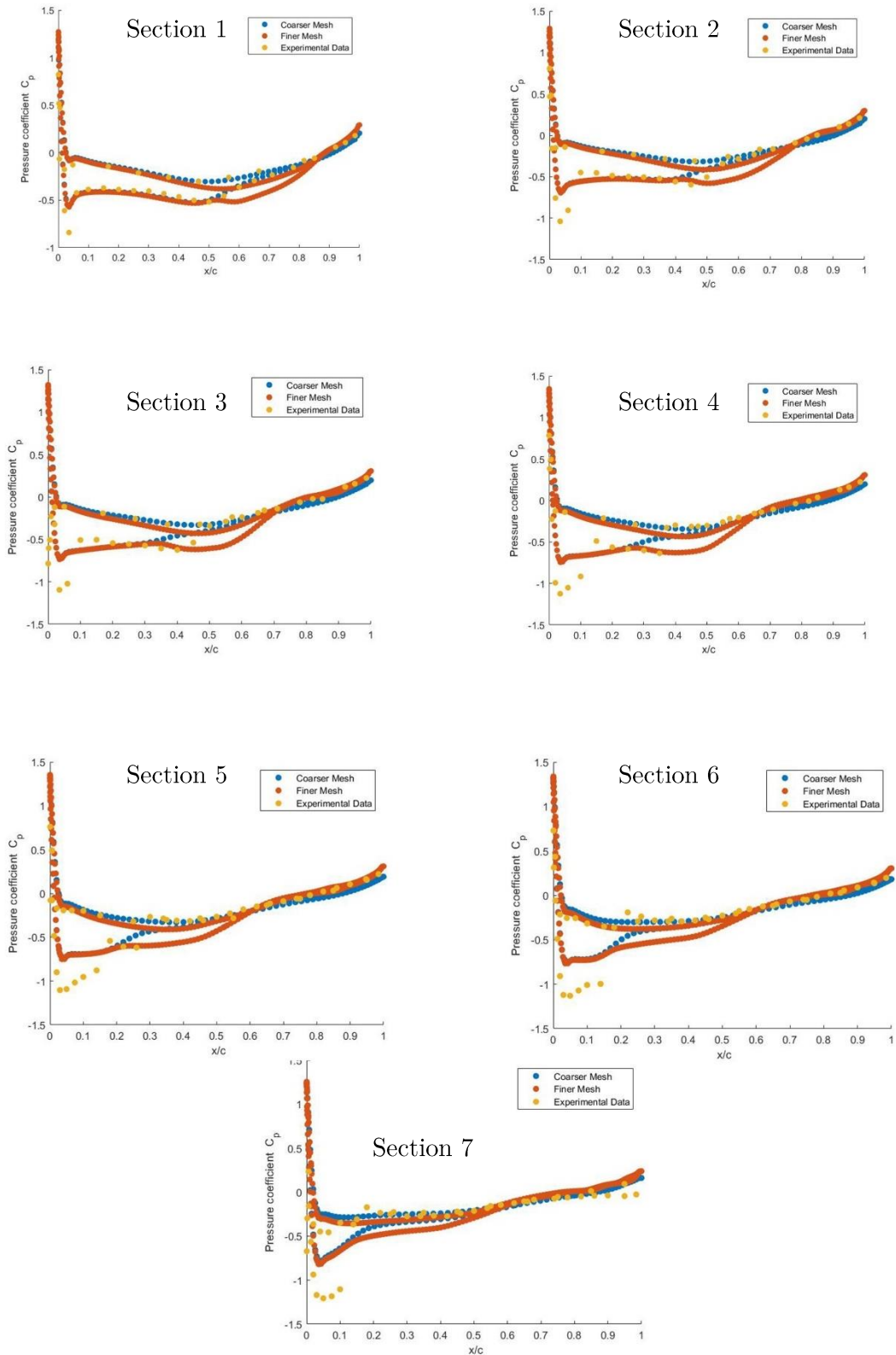


Figure 20. Pressure Coefficient Distribution in Finer Mesh

Additionally, the Mach Contours will be also attached here in case more information from this finer mesh can be added to the phenomena we described in Results. We will recur again to Ansys CFD-Post to represent the results since the problem of grid-like fluid field plot has not been already solved in Ansys-Fluent Software.

Overall, in Figure 21, we can perceive the same phenomena we discussed in the coarser mesh. Both results are really alike. However, little punctualities and differences seen will be commented.

The criteria to represent the colors is with the maximum local Mach computed in the whole simulation, having the red color, to the lowest where blue color is displayed. As it can be seen, here the maximum Mach number is 1.327 instead of the 1.273 from Figure 12. Then, the zones with the same color will actually be more intense here than in the previous graph (Mach number will be higher if colors are conscientiously examined). The supersonic expansion zone will be slightly more intense in the finer mesh than in the coarser one, such as the pressure coefficient distribution - Figure 20- already suggested. Then, according to the shock wave theory, show waves could suffer a little displacement to the tailing edge and boundary layer may also get closer to detachment.

Additionally, in section 3, the expansion zones of same local Mach number are divided into two most intense zones instead of one in the coarser mesh. This fact is singular in this region and has not been sighted in the other sections, then it is primarily bounded to take place between sections 2 and 4 (44 to 80% of the b parameter). This effect could be caused to transitory and spatially dependent mixing layer phenomena of that region, causing both Mach cores not to be united in a single one as expected. Nevertheless, this hypothesis made by the author is weak and the origin of the behavior sighted could be any other.

At last, it can be noted more effect of the vortical structures in the wingtip to the flow over the sections if sections 6 and 7 (the closest to the wingtip) are evaluated. Then, more ability to predict vortical structures can be awaited from the finer mesh. This subject matter will be further discussed in Figure 22 and Figure 23.

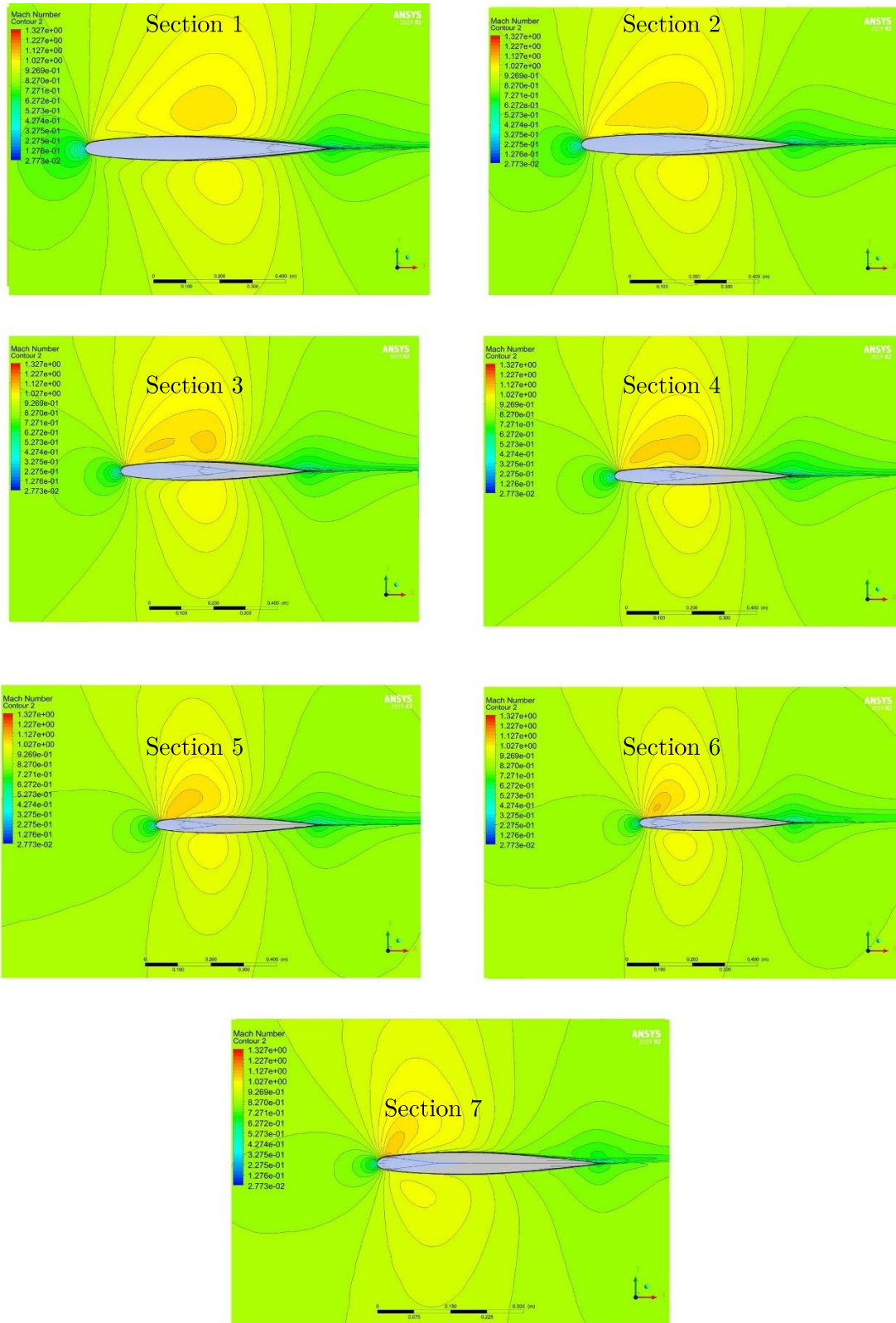


Figure 21. Mach Contours of all sections for Finer Mesh

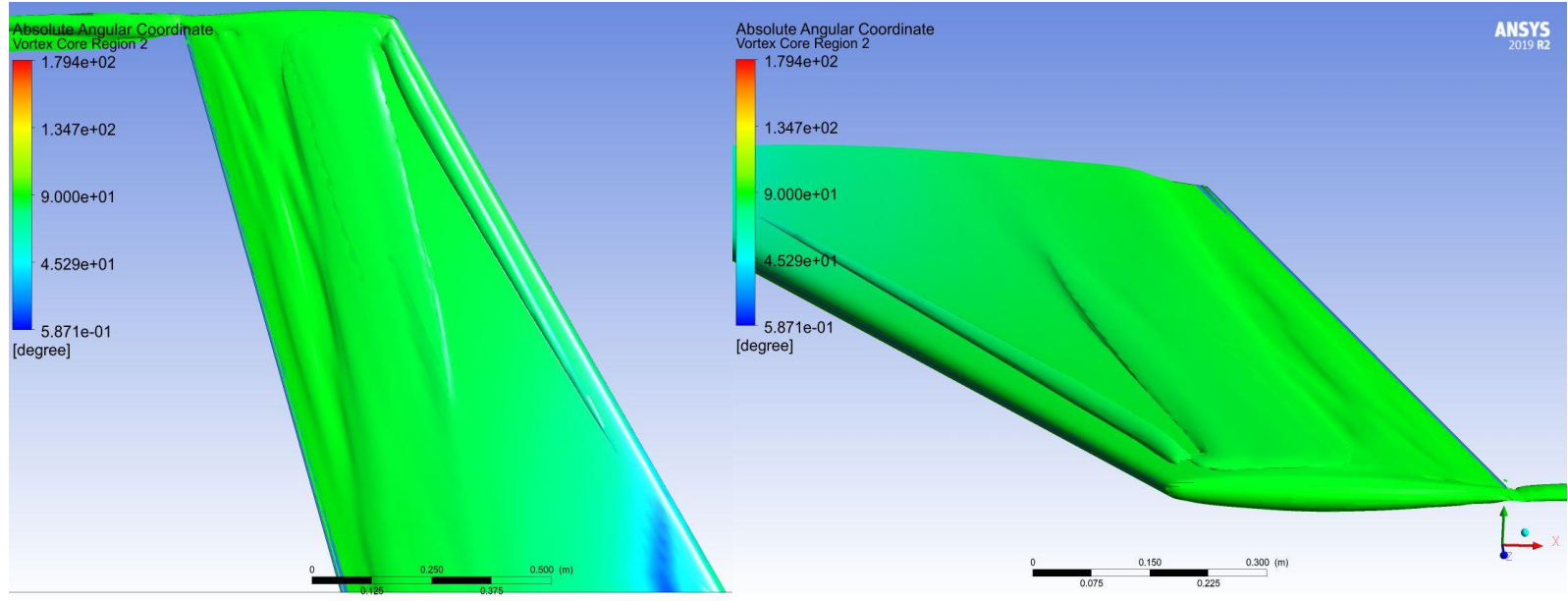


Figure 22. Up and lateral (from the wing tip) perspectives of vortex prediction, Q -criterion $q=0.001$

Figure 19, in contrast with Figure 16, has been able to predict more vortical structures as it was expected; even though it may also be caused to the possible overprediction foreseen in Figure 20. Now, the expansion zones, the shockwave and initial stages of boundary layer detachment can be respectively seen as flow advances from the heading edge of the wing to its tail. Furthermore, in Figure 23 the detail of how the boundary layer thickens due to the shock wave is graphed as it was prognosticated in Aerodynamic Problem.

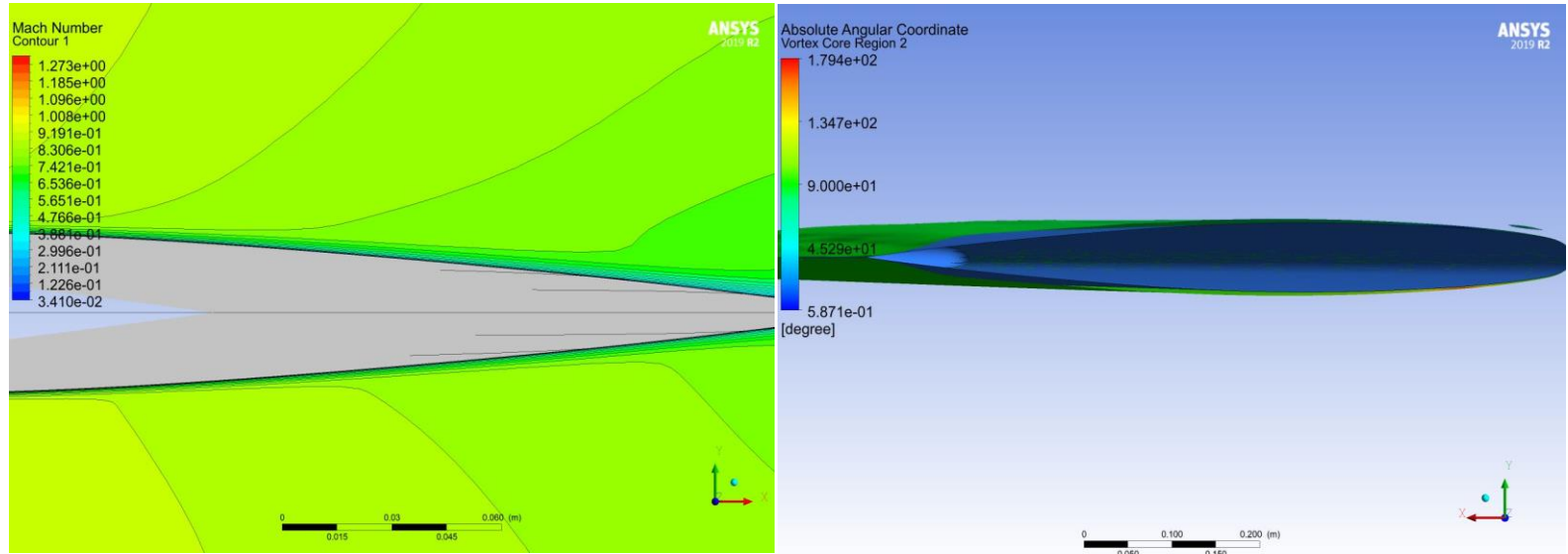


Figure 23. Boundary Layer widening

Appendix 2: Figure Detail

ANSYS
2019 R2
ACADEMIC

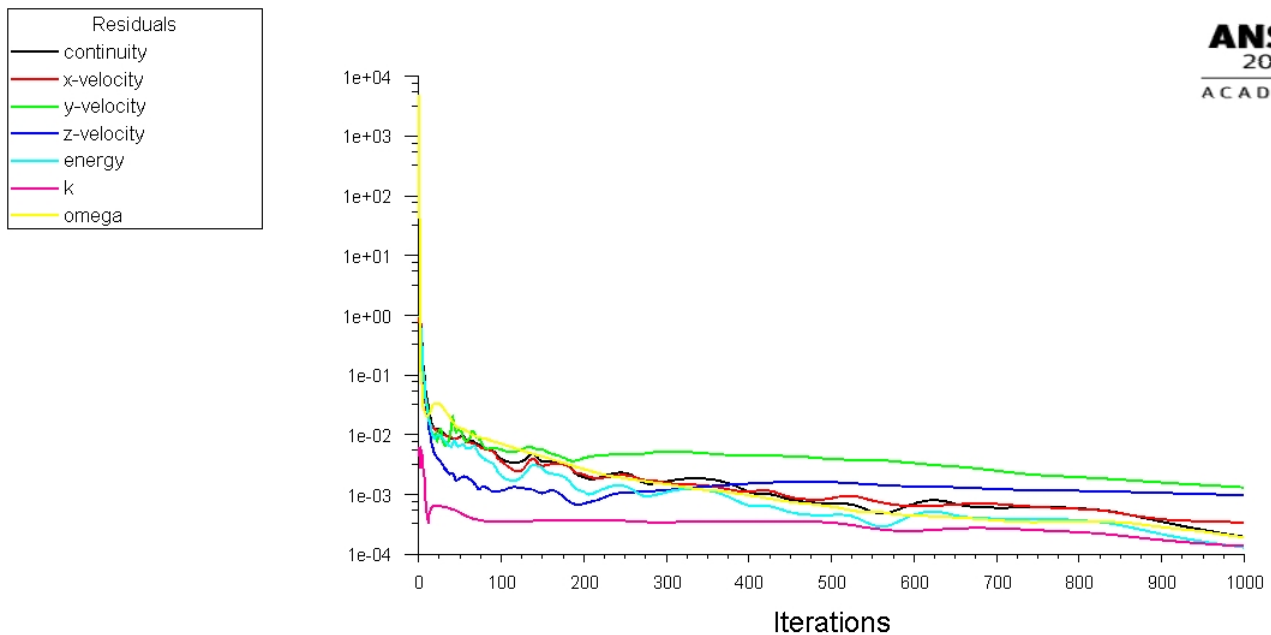


Figure 24. Residuals of the Coarser Mesh

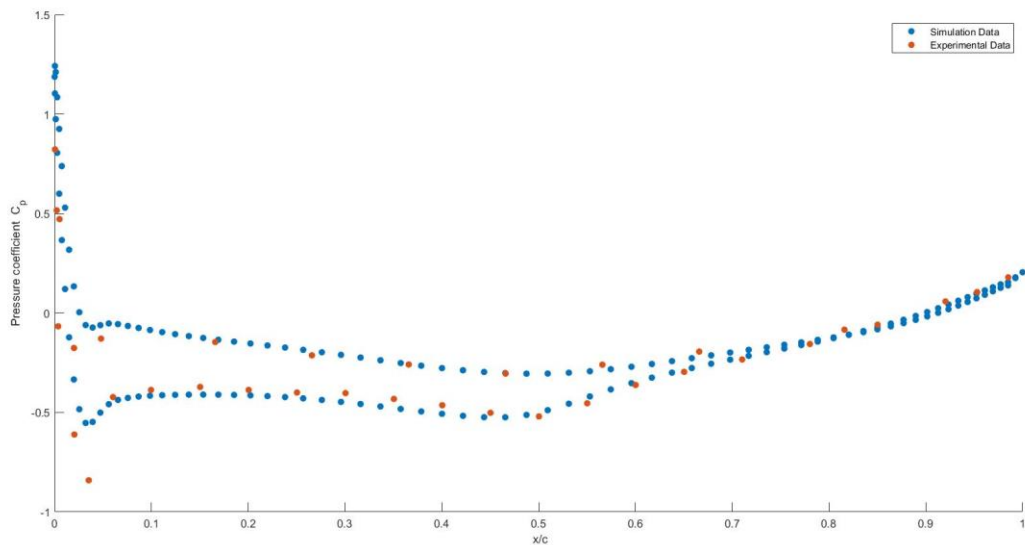


Figure 25. Pressure coefficient distribution for Section 1, Coarse Mesh

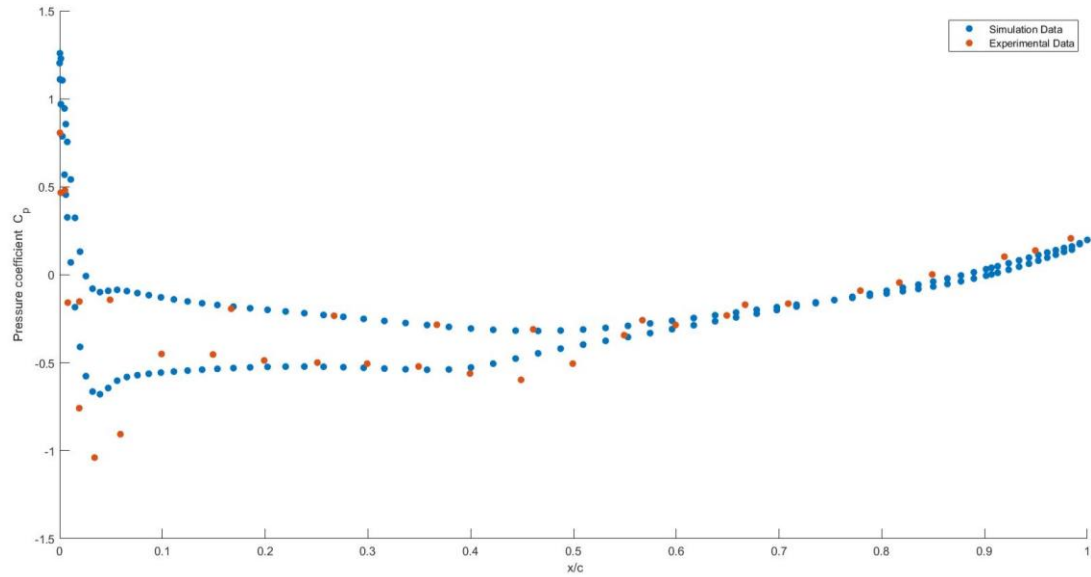


Figure 26. Pressure coefficient distribution for Section 2, Coarse Mesh

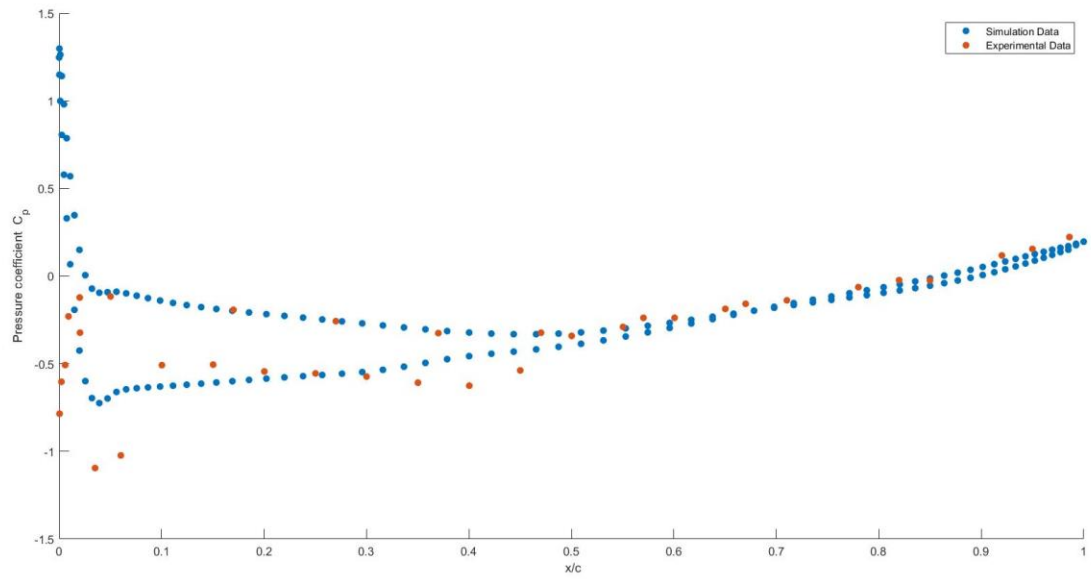


Figure 27. Pressure coefficient distribution for Section 3, Coarse Mesh

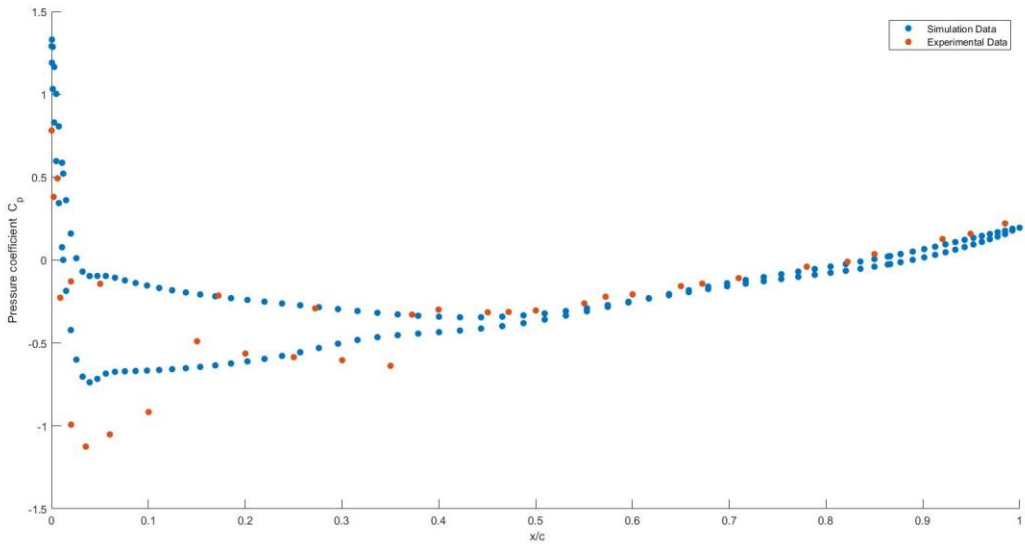


Figure 28. Pressure coefficient distribution for Section 4, Coarse Mesh

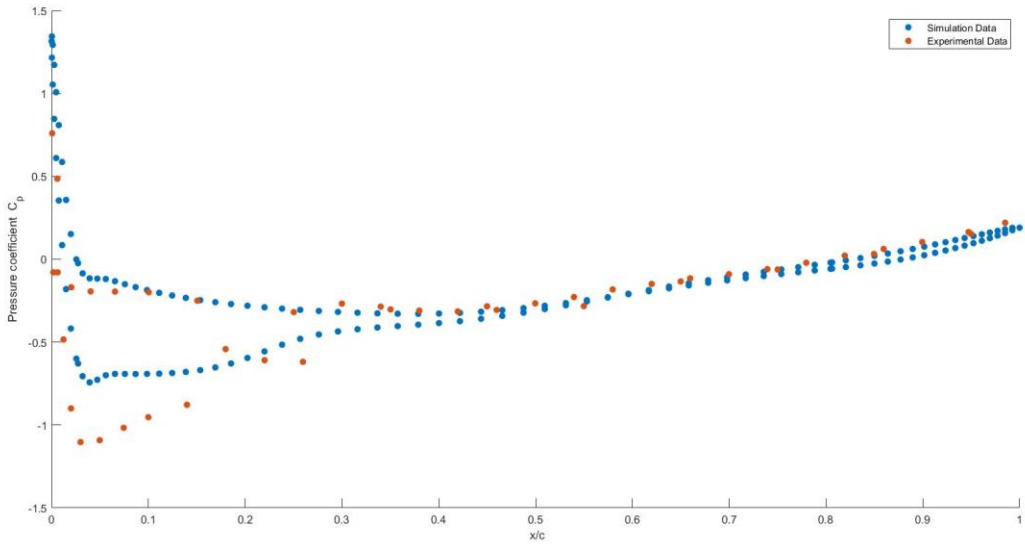


Figure 29. Pressure coefficient distribution for Section 5, Coarse Mesh

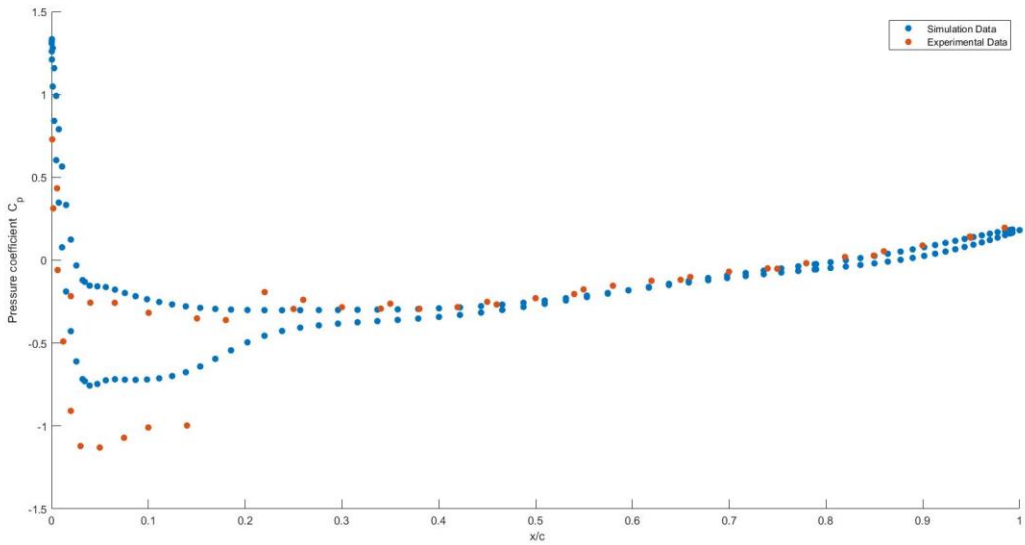


Figure 30. Pressure coefficient distribution for Section 6, Coarse Mesh

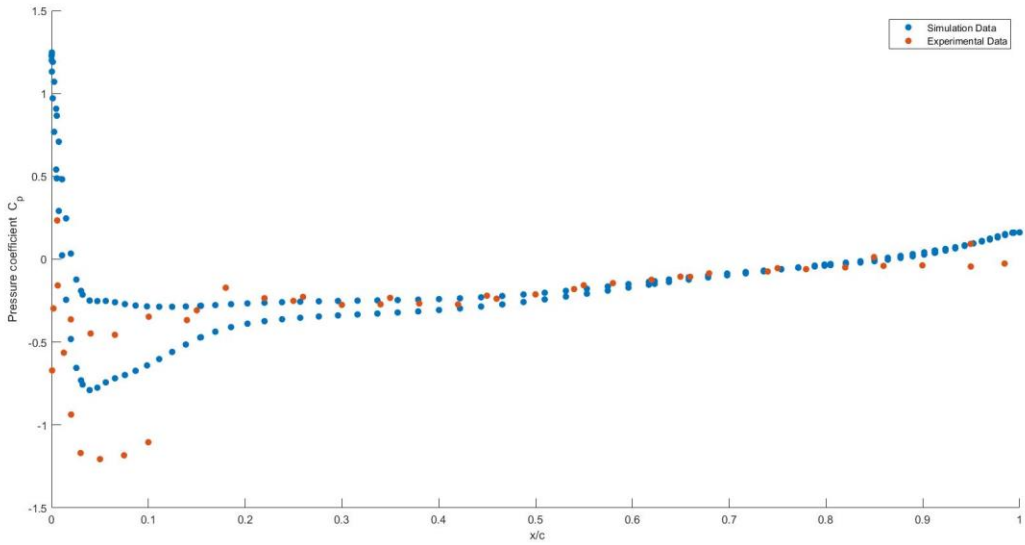


Figure 31. Pressure coefficient distribution for Section 7, Coarse Mesh

**Appendix 3: Digitalized Experimental Data from (SCHMITT and CHARPIN, 1979),
Case 2307.**

SECTION 1		SECTION 2		SECTION 3		SECTION 4		
X/L	CP	X/L	CP	X/L	CP	X/L	CP	
12	0.953	0.105	0.94937	0.138	0.94999	0.155	0.94937	0.16
11	0.81597	-0.084	0.81705	-0.044	0.81986	-0.023	0.82225	-0.009
10	0.66593	-0.194	0.66698	-0.17	0.67008	-0.158	0.67216	-0.141
9	0.56588	-0.26	0.56705	-0.258	0.57033	-0.238	0.5723	-0.22
8	0.46588	-0.305	0.46076	-0.31	0.47037	-0.323	0.4722	-0.312
7	0.3658	-0.259	0.36705	-0.284	0.37009	-0.325	0.37235	-0.328
6	0.26579	-0.213	0.26705	-0.233	0.2701	-0.257	0.2723	-0.29
5	0.16594	-0.146	0.16699	-0.193	0.1701	-0.192	0.17242	-0.213
4	0.04793	-0.129	0.04907	-0.142	0.05016	-0.116	0.05017	-0.142
3	0.02002	-0.176	0.01922	-0.152	0.0201	-0.122	0.01999	-0.128
2	0.00503	0.472	0.0052	0.48	0.00591	-0.507	0.00611	0.494
1	0.00034	0.822	0.00031	0.807	0.00042	-0.785	0	0.783
34	0.00216	0.516	0.00103	0.467	0.00222	-0.603	0.0021	0.382
33	0.00366	-0.067	0.00789	-0.158	0.00914	-0.23	0.00893	-0.226
32	0.02037	-0.611	0.01905	-0.758	0.02036	-0.323	0.02012	-0.992
31	0.03525	-0.841	0.03402	-1.039	0.03508	-1.095	0.0353	-1.124
30	0.06036	-0.423	0.05911	-0.906	0.06022	-1.023	0.06011	-1.051
29	0.09959	-0.387	0.09913	-0.45	0.10029	-0.508	0.10019	-0.916
28	0.15037	-0.372	0.14927	-0.453	0.15032	-0.505	0.15024	-0.489
27	0.20044	-0.387	0.19909	-0.487	0.20029	-0.544	0.20016	-0.563
26	0.25039	-0.4	0.2508	-0.499	0.25024	-0.555	0.25021	-0.585
25	0.3005	-0.403	0.29925	-0.505	0.30008	-0.573	0.30021	-0.603
24	0.3505	-0.432	0.34927	-0.521	0.35024	-0.608	0.35015	-0.637
23	0.40047	-0.464	0.39931	-0.561	0.40037	-0.625	0.39977	-0.298
22	0.4503	-0.502	0.44897	-0.597	0.4501	-0.538	0.45059	-0.314
21	0.50039	-0.52	0.49927	-0.505	0.50024	-0.341	0.5002	-0.303
20	0.55025	-0.454	0.54927	-0.343	0.55042	-0.29	0.55033	-0.26
19	0.60029	-0.362	0.59931	-0.285	0.60071	-0.238	0.60018	-0.206
18	0.65032	-0.296	0.64917	-0.231	0.65026	-0.187	0.65015	-0.156
17	0.71026	-0.234	0.70897	-0.164	0.71034	-0.138	0.70977	-0.108
16	0.78026	-0.156	0.77912	-0.09	0.78008	-0.063	0.78012	-0.039
15	0.85021	-0.059	0.84903	0.002	0.85001	-0.025	0.8501	0.037
14	0.92027	0.058	0.91927	0.103	0.92012	0.118	0.92035	0.128
13	0.98518	0.179	0.98387	0.207	0.98611	0.223	0.98498	0.222

	SECTION 5		SECTION 6		SECTION 7	
	X/L	CP	X/L	CP	X/L	CP
15	0.94977	0.153	0.94953	0.136	0.94946	0.093
	0.84954	0.032	0.84934	0.028	0.84958	0.013
13	0.75003	-0.062	0.74963	-0.051	0.75002	-0.054
12	0.64989	-0.134	0.6498	-0.118	0.64957	-0.105
11	0.54983	-0.283	0.54955	-0.176	0.54967	-0.157
10	0.4498	-0.284	0.44998	-0.251	0.4497	-0.22
9	0.35016	-0.303	0.3499	-0.262	0.34973	-0.233
8	0.25012	-0.319	0.24997	-0.294	0.24976	-0.251
7	0.15054	-0.25	0.15016	-0.351	0.14996	-0.308
6	0.10027	-0.199	0.10019	-0.317	0.10039	-0.347
5	0.0655	-0.195	0.06521	-0.257	0.06536	-0.456
4	0.0403	-0.194	0.03999	-0.256	0.04025	-0.448
3	0.0203	-0.169	0.01985	-0.217	0.01985	-0.363
2	0.00587	0.486	0.00567	0.434	0.00578	0.234
1	0.00057	0.76	0.00068	0.729	0.0005	-0.671
45	0.00184	-0.079	0.0017	0.313	0.00193	-0.297
44	0.00626	-0.079	0.00623	-0.059	0.0063	-0.158
43	0.01228	-0.484	0.01207	-0.49	0.01265	-0.564
42	0.02006	-0.9	0.01983	-0.909	0.02012	-0.937
41	0.02988	-1.103	0.02991	-1.121	0.02999	-1.169
40	0.04966	-1.092	0.04972	-1.13	0.04995	-1.206
39	0.07448	-1.017	0.07483	-1.071	0.07482	-1.183
38	0.09994	-0.953	0.09991	-1.009	0.0999	-1.104
37	0.13986	-0.878	0.13983	-0.997	0.13976	-0.367
36	0.17979	-0.542	0.17999	-0.361	0.17991	-0.172
35	0.22001	-0.609	0.2201	-0.192	0.2199	-0.235
34	0.25964	-0.619	0.25996	-0.239	0.25976	-0.227
33	0.29988	-0.268	0.29994	-0.283	0.29986	-0.275
32	0.33995	-0.286	0.34006	-0.292	0.33979	-0.272
31	0.37986	-0.31	0.37996	-0.293	0.37976	-0.267
30	0.41959	-0.315	0.41938	-0.283	0.41985	-0.273
29	0.45975	-0.306	0.45976	-0.267	0.4597	-0.238
28	0.4996	-0.266	0.49996	-0.229	0.49987	-0.212
27	0.53959	-0.228	0.53988	-0.204	0.53975	-0.18
26	0.57961	-0.182	0.57991	-0.154	0.57985	-0.144
25	0.61987	-0.149	0.6197	-0.124	0.61976	-0.124
24	0.65968	-0.115	0.65979	-0.101	0.65966	-0.106
23	0.6997	-0.09	0.69976	-0.069	0.67919	-0.085
22	0.7394	-0.06	0.7397	-0.049	0.7398	-0.074
21	0.7796	-0.021	0.77962	-0.018	0.77942	-0.06
20	0.81937	0.022	0.81965	0.02	0.81985	-0.049
19	0.85955	0.062	0.8598	0.054	0.85943	-0.04
18	0.8994	0.104	0.89977	0.089	0.89961	-0.037
17	0.94727	0.164	0.94861	0.143	0.94959	-0.044
16	0.98506	0.22	0.98462	0.196	0.98455	-0.026